ANALYSIS OF MULTI-LAYER ARROW PLANAR WAVE GUIDE FOR EVANESCENT FIELD ENHANCEMENT IN LOW-INDEX MEDIA

by

MOHAMMED ABDUL MAJID

A Thesis Presented to the
DEANSHIP OF GRADUATE STUDIES

In Partial Fulfillment of the Requirements
for the Degree

MASTER OF SCIENCE

IN

ELECTRICAL ENGINEERING

KING FAHD UNIVERSITY
OF PETROLEUM AND MINERALS

Dhahran, Saudi Arabia

September 2001

Contents

List of Tables

List of Figures

Nomenclature

English Symbols

$\mathbf{E}$	electric field vector, volts/meter
$\mathbf{H}$	magnetic field vector, amperes/meter
N	diagonal matrix of refractive-index squared at mesh grids
I	identity matrix
P	time-averaged power per unit length in the y-direction, watts/m
Q	matrix of the eigen-value equation
R	reflection coefficient
T	transmission coefficient
n	refractive index
k_o	free space wavenumber, radians/meter
w_0	spot size, micrometer
P_g	guided power, watts/m

P_i	incident power, watts/m
P_t	transmitted power, watts/m
P_r	reflected power, watts/m
x_0	Lateral Position, micrometer
t_c	ARROW core thickness, micrometer
h	mesh size, meter
j	$\sqrt{-1}$
t	time, sec
$\mathbf{A} \cdot \mathbf{B}$	scalar (dot) product of vectors **A** and **B**
$\mathbf{A} \times \mathbf{B}$	vector (cross) product of vectors **A** and **B**

Greek Symbols

ψ	general field component of the **E** or **H** field
Ψ	general field component of the **E** or **H** sampled field, column vector
ϵ_o	free space permittivity, $4\pi \cdot 10^{-7}$ Vs/Am
ϵ_r	relative permittivity
μ_o	free space permeability, $8.8541 \cdot 10^{-12}$ As/Vm
μ_r	relative permeability
$\omega = 2\pi f$	angular frequency, rad/sec
α_m	mth modal field coefficient
χ	Sensitivity

ς	Fraction of Power
$\Delta\Phi$	Phase Difference, degree/millimeter
β	propagation constant. radians/meter
σ	decay factor
λ	wavelength, meter
∇	nabla operator, $\frac{\partial}{\partial x}\hat{a_x} + \frac{\partial}{\partial y}\hat{a_y} + \frac{\partial}{\partial z}\hat{a_z}$
∇^2	Laplace operator, $\frac{\partial^2}{\partial x^2} + \frac{\partial^2}{\partial y^2} + \frac{\partial^2}{\partial z^2}$

Abbreviations

TE	Transverse Electric
TM	Transverse Magnetic
MOL	Method of Lines
OIC	Optical Integrated Circuit
PML	Perfectly Matched Layer
BPM	Beam Propagation Method
CCD	Charged Coupled Device
HIV	Human immuno Deficiency Virus
DNA	Deoxyribonucleic Acid
RNA	Ribonucleic Acid
GOD	Glucose oxidase
GRIN	Gradient Refractive Index

μ TAS	Micro Total Analysis System
ARROW	Anti-resonant Reflecting Optical Waveguide
TIR	Total Internal Reflection
N	Pairs of ARROW Layers
a	thickness of layer, micrometer
d	thickness of layer, micrometer
n_{eff}	Modal Effective Index
Δn_{eff}	Difference between two consecutive Refractive Indices
Re	Real part of a complex number
Im	Imaginary part of a complex number

Subscripts

A_x, A_y, A_z	x, y, z components of a vector $\mathbf{A}$
$\psi_0, \psi_{\pm 1}, \psi_{\pm 2}$	sample number of field ψ
$\psi_{0\pm}, \psi_{1\pm}, \psi_{2\pm}$	field immediately to the left or to the right of a sample point

Superscript

ψ'	first derivative of ψ
ψ''	second derivative of ψ
${n_{eff}}'$	real part of the effective index
${n_{eff}}''$	imaginary part of the effective index
A^*	complex conjugate of A

THESIS ABSTRACT

Name: MOHAMMED ABDUL MAJID

Title: ANALYSIS OF MULTI-LAYER ARROW PLANAR WAVEGUIDE FOR EVANESCENT FIELD ENHANCEMENT IN LOW-INDEX MEDIA

Degree: MASTER OF SCIENCE

Major Field: ELECTRICAL ENGINEERING

Date of Degree: SEPTEMBER 2001

The ARROW (Antiresonant Relecting Optical Waveguide) waveguide is a basic component of integrated optical circuits. In this thesis, multi-layer ARROW planar waveguide is studied for the purpose of enhancing the evanescent field in low-index media. This leads to enhancing the sensitivity of optical detection in the low-index media. We have analyzed this structure using water as the low-index superstrate and investigated different aspects which include a study of the polarization properties, sensitivity and coupling loss using endfire excitation. The sensitivity of optical detection and power enhancement of the evanescent field in the low-index superstrate of the multi-layer ARROW waveguide is sufficiently increased as the the core thickness of the multi-layer ARROW waveguide is decreased. Gaussain beam coupling problem which involves a single discontinuity is successfully analyzed using the Method of Lines (MOL). The Perfectly Matched Layer (PML) absorber is used to absorb the radiated fields from this discontinuities. The MOL with Higher-order approximations of the second derivative ($\partial^2/\partial x^2$) operator with appropriate interface conditions are used in the analysis.

Keywords: ARROW Waveguide, Multi-layer ARROW Waveguide, Evanescent Field Enhancement, Sensitivity, Polarization, Gaussain Beam Coupling, Method of Lines (MOL),Low-index Media, Higher-Order Approximations, Perfectly Matched Layer (PML).

Master of Science Degree

King Fahd University of Petroleum and Minerals, Dhahran.
September 2001

Chapter 1

Introduction

1.1 Integrated Optics

Dielectric waveguides have been studied since the early years of this century. However, the interest in their applications actually started in the sixties. The possibility of guiding light along dielectric layers, has been done experimentally in 1963, which actually stimulated the growth of a new class of passive and active components. The field integrated optics was first proposed in 1969 by S.E Miller of Bell labs [1, 2]. Integrated optics is the name given to opto-electronic systems in which the familiar wires and cables are replaced by light-guiding optical fibres, and conventional integrated circuits are replaced by optical integrated circuits (OICs). In an OIC, the signal is carried by means of a beam of light rather than by an electric current, and the various circuit elements are interconnected on the substrate wafer by optical

waveguides. By combining such layers and shaping them into appropriate configurations, integrated optics technology has realized a large variety of components which can perform a wide range of operations on optical waves. Thus, light can be guided, modulated, deflected, filtered, radiated into space, or by using laser action, it can be generated within thin-film structures.

Two important technical developments gave impetus to this new technology, these are the development of the laser as a source of light that can be manipulated to carry information and the development of the optical fiber as a viable low-loss transmission medium. Some advantages of integrated-optic systems includes reduced weight, much increased bandwidth, immunity to electro-magnetic interference as well as low loss in signal transmission. When the basic components: source, waveguide and detector are all integrated on a single substrate, we have a monolithic OIC. Compound semiconductors such as gallium arsenide ($GaAs$) and indium phosphide (InP) are the candidate substrates for this type of OIC. When the components are made of dissimilar materials, we have a hybrid OIC. For example, the source and detector are made of compound semiconductors such as silicon (Si) and the waveguide is made of dielectric materials such as lithium niobate ($LiNbO_3$) or silica (SiO_2).

Coupling loss is an important design parameter in Optical Fiber Communications and Integrated Optics. There has been a considerable interest during the past two decades in the development of new means of increasing the efficiency of the input and output coupling arrangements. A substantial portion of the light power can

be lost in the region between the waveguide and the open-space or between the IO waveguide and the optical fiber, making the analysis of the factors that influence the coupling efficiency of great importance.

1.2 Optical Waveguides

An optical waveguide is a device which can confine light energy and transport it from one region of space to another with low power loss. A well-known and important example of an optical waveguide is the optical fiber which is a cylindrical waveguide. Usually, total-internal-reflection (TIR) phenomenon is utilized to design such an arrangement. Another example is the dielectric slab waveguide which has a middle layer of high refractive index surrounded by layers of lower refractive indices on both sides. Thus, electromagnetic energy can be trapped inside the high index layer (core) by TIR phenomenon on both sides of the core and can be transported over a long distance. These waveguides could also have a multi-layer structure with more than three layers. The refractive index profile may be uniform (step-index) or continuously varying (graded-index) in each layer.

1.3 ARROW Waveguide

Anti-Resonant Reflecting Optical Waveguides have received much attention due to their attractive features such as low transmission loss, high polarization selectiv-

ity, compatibility with mono-mode optical fibers [3] due to the large core size and small refractive index mismatch. They can be easily integrated monolithically with electronics components as they use SiO_2/Si material system [4]. This makes it a favorable candidate for designing complete integrated optics circuits having all the necessary components, that is: source, waveguide and detector on a single wafer of Silicon. These devices are used in optical communication networks, wavelength selective filters, directional coupler, power splitter, modulator, semiconductor laser sources, detectors and optical sensors.

A typical ARROW waveguide is shown in the figure 1.1. The ARROW structure is characterized by the presence of a high index layer n_2 which provides the high reflectivity required to achieve low loss operation of the waveguide. It is also noted that TE modes of the ARROW waveguide are generally low loss while the TM modes are of high loss [5, 6], since TM reflections are always lower by the same phenomenon which gives rise to the Brewster angle. Therefore,this device also behaves as a TE pass polarizer.

Unlike conventional waveguides that depend on total internal reflection (TIR) phenomenon for guidance of the optical field in a region of high refractive index surrounded by regions of lower refractive index, the ARROW structure partially depends on anti-resonant reflection [7] for guidance in a medium of low refractive index surrounded by a medium of high refractive index. Since TIR at the core-cladding interface may not be realized in this situation, the ARROW structure is essentially a

leaky waveguide [8] and thus ARROW modes have a complex propagation constant. The radiation losses of the leaky waves are reduced by the high reflectivity of an anti-resonant cladding layer.

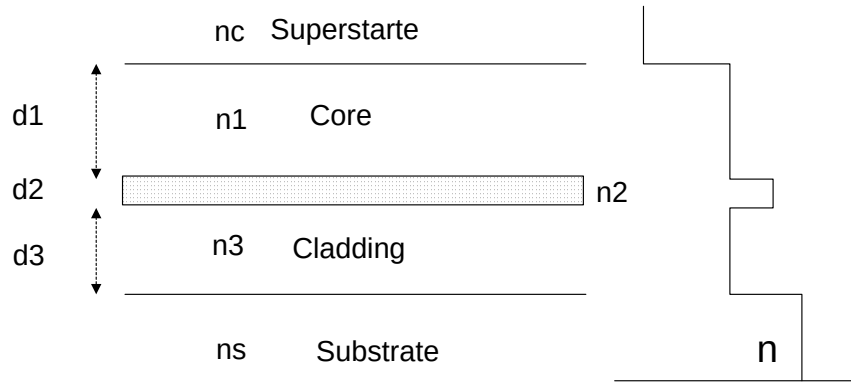

Figure 1.1: Refractive Index Profile in an ARROW Waveguide

1.4 Multi-layer ARROW

Figure 1.2 shows the waveguide structure based on multi-layer ARROW (Anti-resonance Reflecting Optical Waveguide) for sensing operation [9]. It will be shown later that an appropriate choice of design parameters of the proposed structure leads to considerable enhancement of the evanescent field in low index superstrate, while maintaining low leakage loss.

In this work we choose water as the low index superstrate material. The layer immediately below water is made of silica with an assumed refractive index $n_s = 1.46$

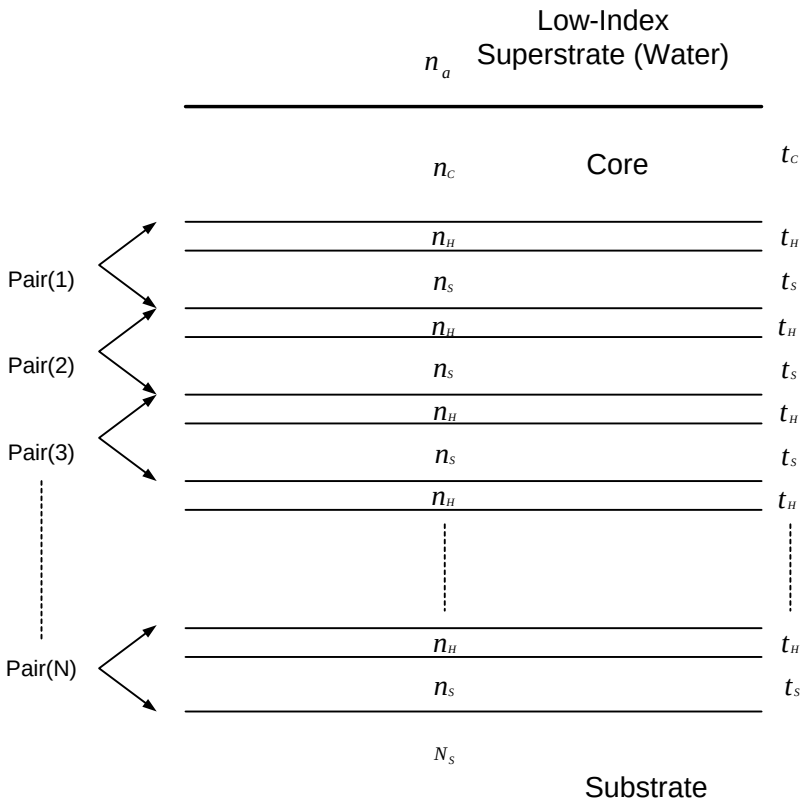

Figure 1.2: Multi-Layer ARROW structure

and thickness t_C . We shall refer to this layer as the core. The layer below the core is made of high index material ($n_H = 2.3$) having thickness t_H. This is an ARROW layer [9] which is used here to cause wave reflection in the vertical direction towards the core layer. The next set of layers consists of a total of N identical pairs of layers. Each pair consists of a silica layer ($n_s = 1.46$) on the top of a high -index ($n_H = 2.3$) ARROW layer. The thickness of the silica and the high-index layers are t_s and t_H respectively. The bottom most layer is the substrate, which is also assumed to be made of silicon dioxide ($SiO2$). When N=1, the total number of layers in the vertical direction is exactly four. This includes the superstrate, the core layer, a single high-index ARROW layer and finally the substrate.

1.5 Method of Lines and other Numerical Methods

Optical waveguide problems that can be analytically solved are limited to simple structures and devices. For complicated devices, either analytical solutions do not exist in closed form or even if they exist, they are difficult to obtain. Several numerical methods have been developed to model longitudinally-varying waveguide structures. Among these methods are the Collocation Method [10], Method of Lines (MOL) [11, 12], Mode Matching Method (MMM) [13], Beam Propagation Method (BPM) [14, 15] and the Finite Difference Time Domain (FDTD) method [16]. These

Methods and other methods are best reviewed in [17, 18]. The basic BPM can not be used to model waveguide discontinuities due to its inability to account for backward reflected waves at a longitudinal discontinuity. It is also an approximate method which requires the wave to be paraxial [13]. The FFT-BPM version is also known to be inefficient in problems having large index discontinuities in the transverse direction. Hence, it is good only for low contrast waveguides and for gradual bends in optical waveguides.

The FDTD method can be used to model longitudinal discontinuity problems but it requires the whole structure to be discretized and stored in computer memory. Hence to model long gratings, the FDTD requires excessively large memory. Also this is a time-domain method and the algorithm should be run for considerable amount of time to get steady state response and some post-processing may be necessary. At any rate this method has gained popularity due to both its ease of understanding and implementation.

The Collocation Method is based on the Helmholtz equation [19]. In this method, the field is expanded into a set of suitable orthogonal basis functions $\phi_n(x)$ in the transverse direction. The choice of basis functions depend on the problem geometry. Since these basis are not eigen-modes of the problem, we need a larger number of basis functions to achieve accurate results.

The Mode Matching Method (MMM) or Eigenmode Propagation Method (EPM) employs eigen-mode expansion of the field, in which the discrete guided modes, the

continuous radiation modes and continuous evanescent modes are taken as basis [20]. The choice of these basis functions is problem dependent. The reflected and transmitted fields are solved through a mode matching procedure.

The Method of Lines (MOL) is a semi-analytical technique used to solve partial differential equations (PDE). For an n-independent variable PDE, only (n-1) variables are discretized to obtain a system of ordinary differential equations (ODE) [21, 22] in the remaining independent variable, which can be solved analytically. This results in a higher numerical accuracy due to the reduced number of discretized variables, less computational time due to the analyticity in the remaining independent variable and smaller memory requirements as we do not need to discretize in the analytical direction. Instead of approximating the field by a series expansion of basis functions (as done in the Mode Matching Method), the second-derivative operator is approximated by a finite-difference scheme. The resulting matrix ODE is solved to find the eigenmodes of the structure. This method can account for backward reflected field due to longitudinally inhomogenous structures, which permits the analysis of planar waveguides having longitudinal discontinuities.

1.6 Statement of the Problem

The Method of Lines is chosen for the analysis of waveguide structures in this thesis, because it is a rigorous method and can model high-contrast waveguides. It

can account for the reflected field at sudden longitudinal waveguide discontinuities, junctions and bends. The basic three-point central-difference approximation of the second derivative operator, which is used in the Method of Lines gives relatively poor estimate of the modal fields and effective indices of a multi-layer waveguide structure. Thus we will use higher-order approximations of the second derivative operator with appropriate interface conditions to improve the accuracy while using fewer discretization lines to sample the problem space. This helps to reduce the computational time required to obtain stationary solutions as well as the analysis of multiple discontinuity problems. Another improvement to MOL is achieved by using a non-uniform meshing scheme to reduce the number of required sampling points. When radiative fields are involved in the problem, we need to terminate the problem space by an appropriate absorbing boundary condition to model an infinite space. In this thesis, a Perfectly-Matched-Layer (PML) [23] is used as an absorbing layer.

MOL will be used to find modal fields and effective indices of the Basic and Multi-layer ARROW(Anti-resonant reflecting optical wave-guide). The ARROW is relatively new waveguide structure and there is much interest in its applications in integrated optics. The Multi-layer ARROW which is to be analyzed in this thesis to understand different aspects of the structure which includes coupling loss of a Gaussian beam using the end fire approach, polarization properties and effects of variations of the real and imaginary parts (sensitivity) of the refractive index of the

low-index superstrate on the optical properties of the fundamental TE mode of the structure. This includes calculations of the acquired phase difference and modal attenuation due to variation of the complex refractive index of the superstrate.

In this thesis we will study different sensing application based on evanescent field which includes Chemical sensing, biochemical and Biosensing. A special device called Biochip will be discussed. We will also study the Bio part of biosensing and some basics of medical field will be explained in conjunction with the optical part for better understanding.

1.7 Thesis Organization

This thesis is organized with a view to present the work from the basic slab waveguide theory to the discussion of results obtained from our study of a multi-layer planar waveguide. This thesis consists of seven chapters. In chapter 1, a basic overview of Integrated Optics, Optical Waveguides, ARROW waveguide, Multi-Layer ARROW Waveguide and Method of Lines is given.

Theory of the dielectric slab waveguide is presented in chapter 2, because the fundamental component of guided-wave opto-electronic devices is the optical waveguide, which supports the optical field. This chapter starts by introducing Maxwell's equations. By using Maxwell's equation, the wave equation is obtained and subsequently used to analyze the stationary modes of a slab waveguide.

Chapter 3 starts with the introduction of the Method of Lines (MOL), which is applied to solve the scalar wave equation. The three-point central difference approximation of the second derivative operator is introduced, the five point and the seven point approximation with appropriate interface conditions are briefly discussed. Exact results are compared to the numerical based on the MOL in order to establish the accuracy of the MOL.

In Chapter 4, the Anti-Resonant Reflecting Optical Waveguide (ARROW) is described and the Method of Lines is used to model this structure. The effective indices and modal fields of the ARROW waveguide structure are calculated and compared with analytical results.

In Chapter 5, the Multi-Layer Planar Waveguide is introduced. Evanescent Field Enhancement, polarization properties, effects of variations of the real and imaginary parts (sensitivity) of the refractive index of the low-index superstrate on the optical properties of the fundamental TE mode of the structure (This includes calculations of the acquired phase difference and modal attenuation due to variation of the complex refractive index of the superstrate) are calculated and discussed.

Chapter 6, starts with the introduction of the application of evanescent field enhancement in low index-supertsrate. Different sensing applications based on evanescent field which includes chemical sensing, biochemical and biosensing are discussed. The concept of the Biochip is introduced and some basics of medical field are discussed in conjunction with the optical part.

Chapter 7, introduces the basic formulation for the MOL analysis of Gaussian beam coupling to the multi-Layer ARROW waveguide which includes, coupling techniques, calculation of power coupling efficiency in edge coupling, the application of the MOL to the coupling problem, calculation of power coupling efficiency using the MOL. The coupling loss of a Gaussian beam using the end fire approach is presented with the results given at the end of the chapter.

In the last chapter, this work presented is summarized along with conclusions and few possible future extensions are proposed.

Chapter 2

Dielectric Slab Optical Waveguide

2.1 Introduction

The simplest of the optical waveguides is the Dielectric slab waveguide. Because of its simple geometry, radiation modes and guided modes (A mode is a transverse field profile that retains the same shape (except for attenuation)as the field propagates along the guide) can be described by simple mathematical expressions. In gaining understanding of the more complicated dielectric waveguide properties study of simple slab waveguide is essential. It must be noted, that slab waveguides are not only useful as models for more general types of optical waveguides but they are actually employed for light guidance in integrated optical circuits [24, 25, 26, 27, 28].

In this chapter, the theory of planar dielectric waveguides will be explained. Starting with Maxwell's equations, we will give a brief description of the propagation of

optical modes in slab waveguide.

2.1.1 Basic Formulation

Figure 2.1 shows a schematic diagram of a three-layer planar waveguide. The core region of the waveguide, which is also called the film, is assumed to have a refractive index n_1. The film is deposited on a layer called the substrate which has a refractive index n_2. The cladding on the film is called the superstrate which has a refractive index n_3.

In this section, we will consider the stationary modes of the basic three-layer dielectric slab waveguide. This structure is an asymmetric dielectric slab waveguide, shown in figure 2.2. As can be seen, this figure shows a longitudinal cross-section of the slab waveguide shown in figure 2.1. In figure 2.2, we assume that the dimension of the slab along the y-axis is considerably larger than its dimension along the x-axis and that no material or field variation exist along the y-direction. Such a waveguide supports a finite number of guided modes as well as an infinite number of unguided radiation modes. Assuming that $n_1 > n_2 \geq n_3$, it follows that total internal reflection (TIR) can occur at both interfaces. It should be noted that the number of guided modes that can be supported by a slab waveguide depends on the thickness $2a$, the wavelength λ and the indices of refraction, n_1, n_2 and n_3. starting with Maxwell's equations in a source-free region in terms of the refractive index n_i $(i = 1, 2, 3)$ of the three layers and assuming that the material of each layer is

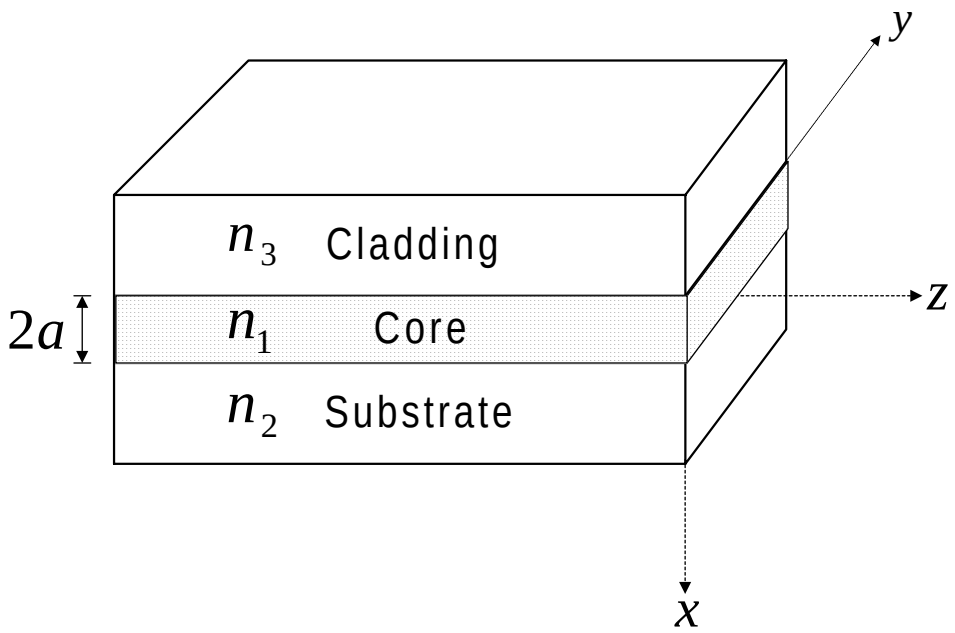

Figure 2.1: Schematic Diagram of A Dielectric Slab Waveguide

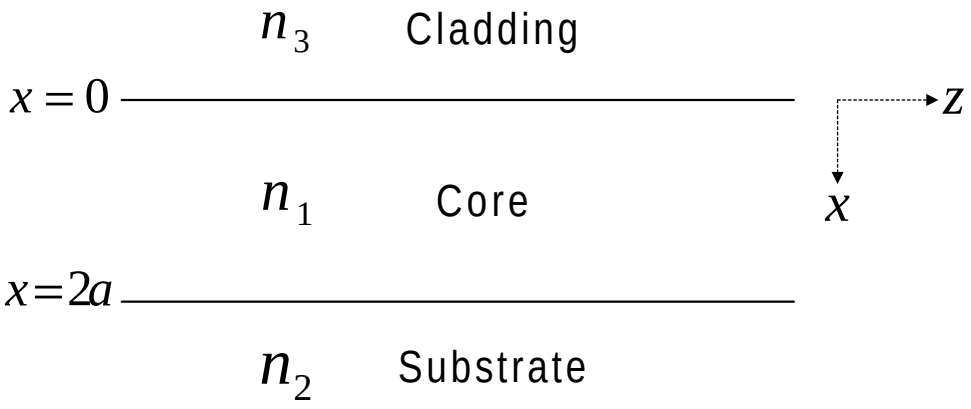

Figure 2.2: A Three-Layer Dielectric Slab Waveguide, 2D view

non-magnetic, homogeneous and isotropic (these assumptions are valid throughout this thesis), that is $\mu = \mu_o$ and ϵ is uniform and scalar, we have [24]:

$$\nabla \times \mathbf{E} = -\mu_o \frac{\partial \mathbf{H}}{\partial t} \tag{2.1}$$

$$\nabla \times \mathbf{H} = n_i^2 \epsilon_o \frac{\partial \mathbf{E}}{\partial t} \tag{2.2}$$

$$\nabla \cdot \mathbf{E} = 0 \tag{2.3}$$

$$\nabla \cdot \mathbf{H} = 0 \tag{2.4}$$

To obtain the above equations, we used $\mathbf{D} = \epsilon \mathbf{E} = n^2 \epsilon_o \mathbf{E}$, $\mathbf{B} = \mu_o \mathbf{H}$, $\mathbf{J} = 0$.

If we apply the curl operator to equation 2.1, we get:

$$\nabla \times \nabla \times \mathbf{E} = -\mu_o \nabla \times \frac{\partial \mathbf{H}}{\partial t} \tag{2.5}$$

$$= -\mu_o n_i^2 \epsilon_o \frac{\partial^2 \mathbf{E}}{\partial t^2} \tag{2.6}$$

where equation 2.2 has been used to eliminate $\mathbf{H}$. To simplify further, we use the vector identity

$$\nabla \times \nabla \times \mathbf{A} = \nabla(\nabla \cdot \mathbf{A}) - \nabla^2 \mathbf{A} \tag{2.7}$$

where $\mathbf{A}$ is an arbitrary vector field. Using equations 2.3 and 2.7, equation 2.6 can

be simplified to:

$$\nabla^2 \mathbf{E} = \mu_o \epsilon_o n_i^2 \frac{\partial^2 \mathbf{E}}{\partial t^2} \tag{2.8}$$

Writing the above equation in phasor notation (assuming a time-harmonic field of the form $e^{-j\omega t}$) we obtain [24, 25]:

$$\nabla^2 \mathbf{E} + k_o^2 n_i^2 \mathbf{E} = 0 \tag{2.9}$$

which is the familiar three-dimensional vector wave equation for a uniform dielectric with refractive index n_i. Here k_o is the free-space wave number given by $k_o = \omega\sqrt{\mu_o \epsilon_o}$. The electric field vector $\mathbf{E}$ in equation 2.9 is a phasor quantity, which is complex and has both a magnitude and a phase. In addition, $\mathbf{E}$ is in general a function of space co-ordinates x, y, z and angular frequency ω. $\mathbf{E}$ is independent of time since the time dependence has been removed by the phasor transformation. We may simplify equation 2.9 by assuming that the structure is uniform in the y-direction (see Figure 2.1) and extends to infinity in the y-direction. This allows us to assume that the field $\mathbf{E}$ is also uniform in this direction. Thus $\frac{\partial}{\partial y}$ is replaced by zero. If we further assume a z-dependence of the form $e^{j\beta z}$, with β as the longitudinal propagation constant, Equation 2.9 is simplified and takes the form:

$$\frac{d^2\mathbf{E}}{dx^2} + (k_o^2 n_i^2 - \beta^2)\mathbf{E} = 0 \tag{2.10}$$

The above equation is known as Helmholtz equation. In this case $\mathbf{E}$ is a function of x only and the equation is a second order ordinary differential equation. The propagation constant β can be expressed as $\beta = k_o n_{eff}$, where n_{eff} is called the effective index. The field of a slab waveguide is in general a superposition of Transverse Electric (TE) polarized field and Transverse Magnetic (TM) polarized field. The field components of the two polarizations are H_x, E_y and H_z for TE-polarized waves and E_x, H_y and E_z for TM-polarized waves.

2.2 Transverse Electric (TE) Guided Modes

By using equation 2.10, the TE scalar wave equation and Maxwell's equations [29], for guided mode then applying the boundry conditions at $x = 0$ and at $x = 2d$ to the solution of E_y and H_z in the three regions and eliminating the arbitrary constants [24, 25, 29]: we get

$$\tan(2dq) = \frac{q(p+r)}{q^2 - pr} \tag{2.11}$$

where $r^2 = \beta^2 - k_o^2 n_3^2$, $q^2 = k_o^2 n_1^2 - \beta^2$ and $p^2 = \beta^2 - k_o^2 n_2^2$. This is the eigenvalue equation for the TE modes of the asymmetric slab waveguide. Equation 2.11 is an

implicit relationship which involves the wavelength, refractive indices of the layers and core thickness as known quantities, and the propagation constant β as the only unknown quantity. It can be shown that only certain discrete values of β can satisfy the above equation, so this waveguide will only support a *discrete* set of guided modes. The symmetric waveguide ($n_2 = n_3$) can only support modes with even or odd electric field patterns. In this case it can be easily shown that the eigen-value equation 2.11 reduces to ($p = r$):

$$\tan(2dq) = \frac{2pq}{q^2 - p^2} \tag{2.12}$$

An example of the field pattern of the TE modes for a three-layer slab waveguide is given in figure 2.3. From the figure one can infer that TE_0 is tranverse field profile which does't crosses the axis, but the higher order modes such as TE_1 cross once, TE_2 crosses twice and so on.

2.3 Transverse Magnetic (TM) Guided Modes

The wave equation for this polarization is obtained in terms of the magnetic field component H_y. Using scalar wave equation2.10 and Maxwell's equation [29], and applying boundry conditions at $x = 0$ and at $x = 2d$ to the solution of H_y and E_z in the three regions [24, 25, 29]: we get

$$\tan(2dq) = \frac{qn_1^2\left(n_3^2p + n_2^2r\right)}{n_2^2n_3^2q^2 - n_1^4pr} \tag{2.13}$$

which is the eigenvalue equation for TM modes of an asymmetric slab waveguide. For symmetric case eqauation 2.13 reduces to:

$$\tan(2dq) = \frac{n_1^4 2pq}{n_2^4q^2 - n_1^4p^2} \tag{2.14}$$

An example of the TM mode patterns for a symmetric slab waveguide is given in figure 2.4. As evident from the figure, H_y is continuous across a layer interface but its derivative is discontinuous there, causing a sudden change in the slope of H_y.

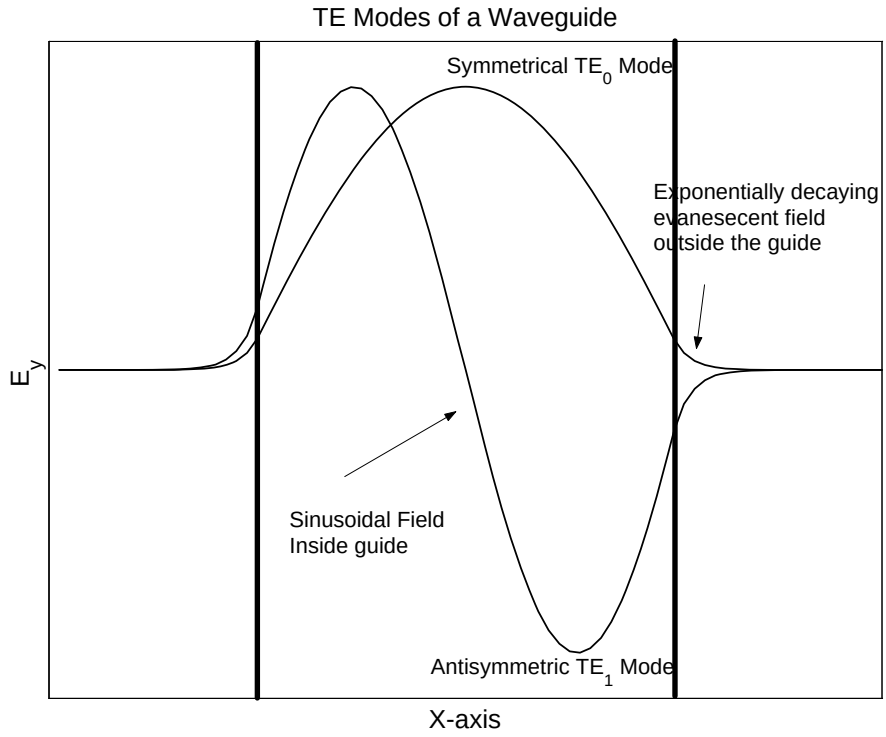

Figure 2.3: TE Mode Patterns of a Symmetric Slab Waveguide

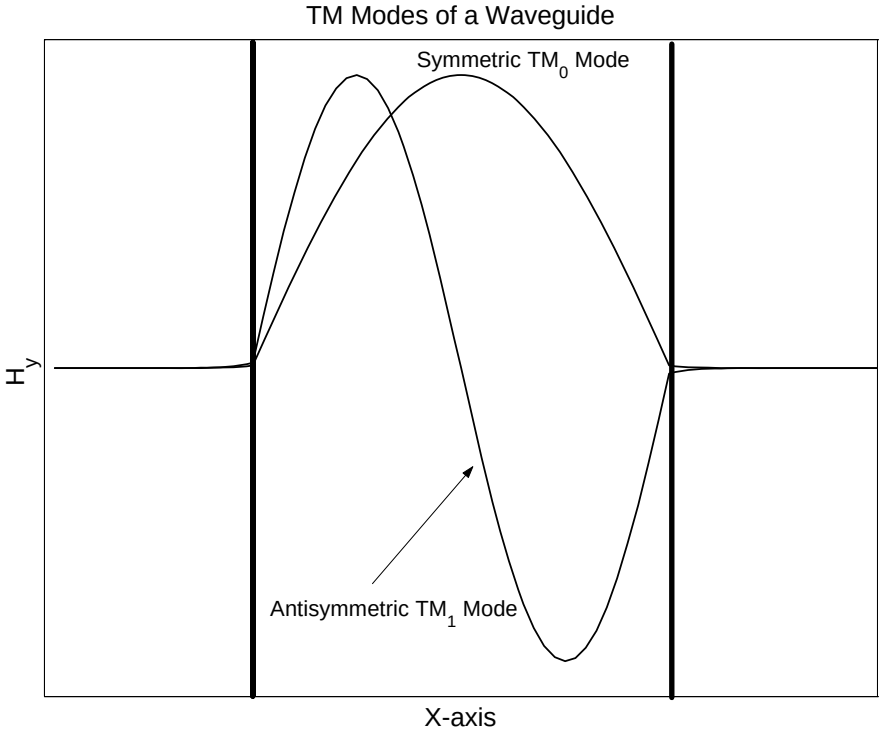

Figure 2.4: TM Mode Patterns of a Symmetric Slab Waveguide

Chapter 3

The Method of Lines

3.1 Introduction

For the analysis of optical waveguide structures various numerical algorithms have been proposed and successfully implemented. One of these methods is the method of lines (MOL),is a semi-analytical technique which results in higher accuracy, less computational time and smaller storage requirement. The MOL has been applied to several types of planar longitudinally uniform waveguide problems. It has been used to analyze single [30, 31] and multiple discontinuities in optical waveguides [11, 22, 32, 33, 34, 35, 36]and to solve non-linear waveguide problems [37] as well as diffraction problems from waveguide ends [38]. It had been successfully used to model 3-D problems [39, 40, 41] for both optical and microwave wave-guides. The method in general has been applied in other branches of science as well.

3.2 Basic Algorithm

When the MOL is applied to two dimensional structures, the waveguide geometry is discretized in the transverse direction (the direction normal to the direction of propagation) and calculated analytically in the longitudinal direction [36](direction of propagation). Figure 3.1 shows a planar waveguide structure in which the interfaces of layers are parallel to the z-axis. Discretization is done in the x-direction. This implies that the field will be calculated on lines that are equidistant from each other and parallel to the z-axis. In some cases it is better to a have non-equidistant discretization (i.e., non-uniform). In locations where the field changes rapidly we can use more lines per unit length whereas in locations where the filed changes slowly we can use few lines. This approach improves the computational time and memory requirement. The computational window is bounded by an electric wall where $E_y = 0$ or a magnetic wall where $H_y = 0$ as appropriate. It must be noted that discretization is done in one coordinate and calculated analytically in the other coordinate. Consider the two dimensional wave equation:

$$\frac{\partial^2 \psi(x,z)}{\partial x^2} + \frac{\partial^2 \psi(x,z)}{\partial z^2} + k_o^2 n^2 \psi(x,z) = 0 \tag{3.1}$$

The $\frac{\partial^2}{\partial x^2}$ term in equation 3.1 is replaced by a three-point central difference approximation of the form:

$$\frac{\partial^2 \psi_i}{\partial x^2} = \frac{\psi_{i+1} - 2\psi_i + \psi_{i-1}}{(\Delta x)^2} \tag{3.2}$$

For detail formulation refer to [29]: At the ith grid we get

$$\frac{\psi_{i+1}(z) - 2\psi_i(z) + \psi_{i-1}(z)}{(\Delta x)^2} + \frac{d^2\psi_i(z)}{dz^2} + k_o^2 n_i^2 \psi_i(z) = 0 \tag{3.3}$$

If the field in the x-direction is discretized into M points, then Equation 3.3 results in the following M equations:

$$i = 1: \qquad \frac{1}{(\Delta x)^2}\left[\psi_2 - 2\psi_1 + \psi_0\right] + \frac{d^2}{dz^2}\left[\psi_1\right] + k_o^2 n_1^2 \left[\psi_1\right] = 0 \tag{3.4}$$

$$i = 2: \qquad \frac{1}{(\Delta x)^2}\left[\psi_3 - 2\psi_2 + \psi_1\right] + \frac{d^2}{dz^2}\left[\psi_2\right] + k_o^2 n_2^2 \left[\psi_2\right] = 0 \tag{3.5}$$

$$i = 3: \qquad \frac{1}{(\Delta x)^2}\left[\psi_4 - 2\psi_3 + \psi_2\right] + \frac{d^2}{dz^2}\left[\psi_3\right] + k_o^2 n_3^2 \left[\psi_3\right] = 0 \tag{3.6}$$

$$\vdots$$

$$i = M: \qquad \frac{1}{(\Delta x)^2}\left[\psi_{M+1} - 2\psi_M + \psi_{M-1}\right] + \frac{d^2}{dz^2}\left[\psi_M\right] + k_o^2 n_M^2 \left[\psi_M\right] = 0 \tag{3.7}$$

The above equations can be written in matrix form as:

$$\frac{1}{(\Delta x)^2}\begin{bmatrix} -2 & 1 & & & & & \\ 1 & -2 & 1 & & & \mathcal{O} & \\ & 1 & -2 & 1 & & & \\ & & \ddots & \ddots & \ddots & & \\ & \mathcal{O} & & & 1 & -2 & 1 \\ & & & & & 1 & -2 \end{bmatrix}\begin{bmatrix} \psi_1(z) \\ \psi_2(z) \\ \psi_3(z) \\ \vdots \\ \vdots \\ \psi_M(z) \end{bmatrix} + \frac{d^2}{dz^2}\begin{bmatrix} \psi_1(z) \\ \psi_2(z) \\ \psi_3(z) \\ \vdots \\ \vdots \\ \psi_M(z) \end{bmatrix}$$

$$+k_o^2\begin{bmatrix} n_1^2 & & & & & & \\ & n_2^2 & & & & \mathcal{O} & \\ & & n_3^2 & & & & \\ & & & \ddots & & & \\ & \mathcal{O} & & & \ddots & & \\ & & & & & & n_M^2 \end{bmatrix}\begin{bmatrix} \psi_1(z) \\ \psi_2(z) \\ \psi_3(z) \\ \vdots \\ \vdots \\ \psi_M(z) \end{bmatrix} = \begin{bmatrix} 0 \\ 0 \\ 0 \\ \vdots \\ \vdots \\ 0 \end{bmatrix}$$

written in a compact notation, we get:

$$\frac{1}{(\Delta x)^2} C\Psi + \frac{d^2}{dz^2}\Psi + k_o^2 N\Psi = 0 \tag{3.8}$$

where C is a tri-diagonal second-order central-difference matrix, N is a diagonal matrix whose elements are $n_1^2, n_2^2, ..., n_M^2$ and $\Psi = [\psi_1(z), \psi_2(z), ..., \psi_M(z)]^t$ is the

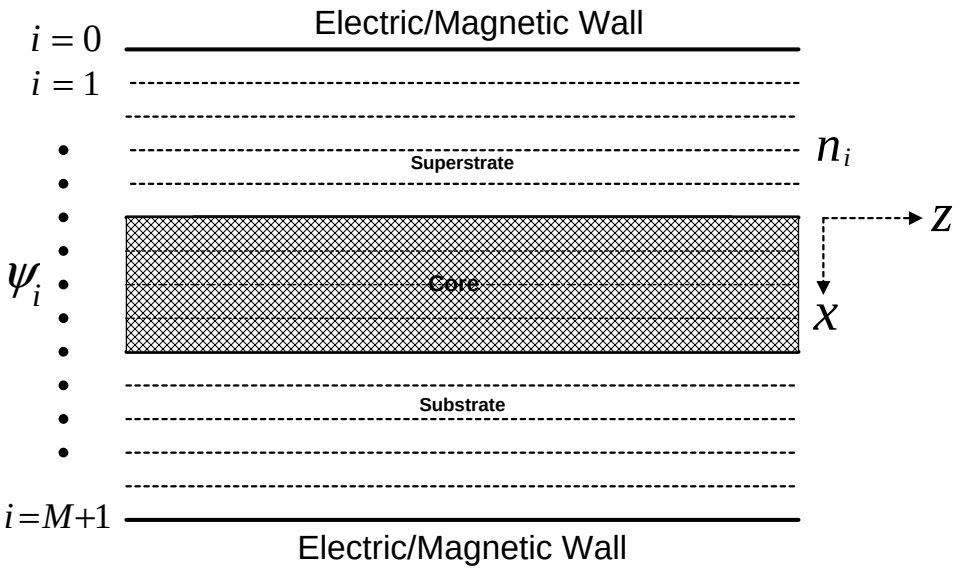

Figure 3.1: Mesh Discretization used in the MOL

discretized field vector. we can define Q as:

$$Q = \frac{1}{(\Delta x)^2} C + k_o^2 N \tag{3.9}$$

Equation 3.8 can be modified as:

$$\frac{d^2}{dz^2}\Psi + Q\Psi = 0 \tag{3.10}$$

This is a 2nd-order differential equation whose solution is given by [11]:

$$\Psi = e^{j\sqrt{Q}z} A + e^{-j\sqrt{Q}z} B \tag{3.11}$$

where $e^{j\sqrt{Q}z}$ represents field propagation in the $+z$ direction and $e^{-j\sqrt{Q}z}$ represents field propagation in $-z$ direction. Substituting $z = 0$, in equation 3.11 results in

$$\Psi = A + B \tag{3.12}$$

This means that the $M \times 1$ column matrix A represents the incident field at $z = 0$, while the matrix B represents the reflected field at $z = 0$. The matrices $e^{j\sqrt{Q}z}$ and $e^{-j\sqrt{Q}z}$ are calculated by diagonalizing the matrix Q to find the eigenvalues and eigenvectors. The matrix Q may then be written in the form:

$$Q = UVU^{-1} \tag{3.13}$$

where U is the eigenvector matrix and V is a diagonal matrix containing the eigenvalues of Q. The matrix exponential can be found using the well known relation of linear algebra:

$$e^{j\sqrt{Q}z} = Ue^{j\sqrt{V}z}U^{-1} \tag{3.14}$$

3.3 Interface Conditions

In order to correctly model the electric and magnetic fields behaviour at an interface, the interface conditions (I.Cs.) should be appropriately accounted for in the Method

of Lines formulation. The tangential electric field E_y and its first derivative are continuous across an interface. For TE polarization the interface condition are given by (for detail formulation refer to) [29]:

$$E_y^{0^+} = E_y^{0^-} \tag{3.15}$$

$$\frac{\partial E_y^{0^+}}{\partial x} = \frac{\partial E_y^{0^-}}{\partial x} \tag{3.16}$$

The tangential magnetic field H_y is continuous but its first derivative is discontinuous at an interface. For TM polarization the interface conditions are given by:

$$H_y^{0^+} = H_y^{0^-} \tag{3.17}$$

$$\frac{1}{n_2^2}\frac{\partial H_y^{0^+}}{\partial x} = \frac{1}{n_1^2}\frac{\partial H_y^{0^-}}{\partial x} \tag{3.18}$$

Where $n1$ and $n2$ are refractive indices shown in figure 3.2

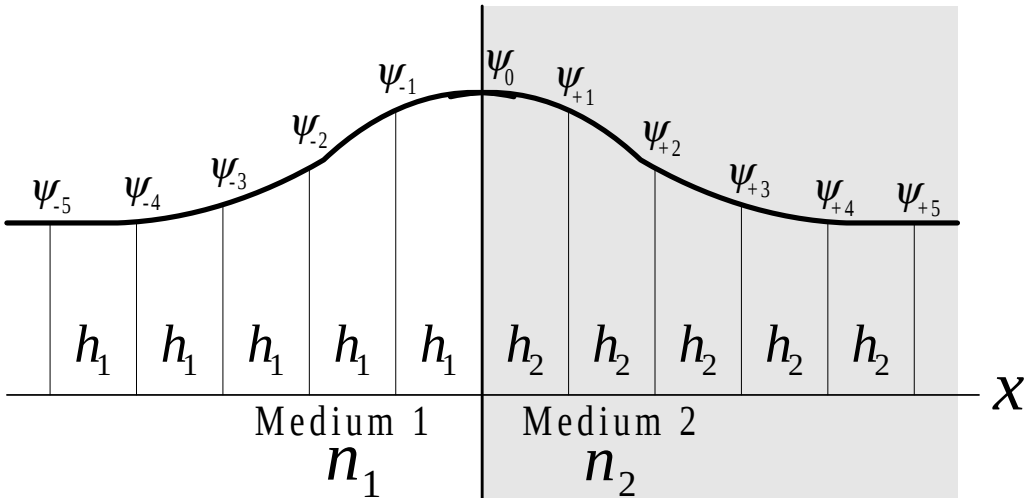

Figure 3.2: Discretized Field in the Transverse Direction

3.4 Higher-Order Approximation of the $\frac{\partial^2}{\partial x^2}$ Operator

In this section we will briefly discuss improvements of the three-point formulation with interface conditions for detail refer reference [29, 22]. The improved formula is given by:

$$\psi''_{0^-} = \frac{\psi_{+1} - (\tau_{21}\rho_{21} + 1 + 0.5h_2^2\zeta_{12})\,\psi_0 + \tau_{21}\rho_{21}\psi_{-1}}{0.5h_2(h_1\rho_{21} + h_2)} \tag{3.19}$$

where $\tau_{21} = \frac{h_2}{h_1}$ (h is mesh size). This relation approximates the $\frac{\partial^2}{\partial x^2}$ operator at any sampling point i in terms of the field values at $i+1$, i and $i-1$ sampling points. So this is a better three-point central-difference approximation of $\frac{\partial^2}{\partial x^2}$ operator since it

accounts for the field at interface boundary conditions. In addition, the non-uniform mesh makes this formulation very efficient.

The improved formula 3.19 for the second derivative approximation has an accuracy of $O(h^2)$ at regions of uniform index and mesh size. Its accuracy decreases at a mesh or index discontinuity. In integrated optical waveguide modeling, the required accuracy in estimating the effective index is fairly high. So we need to use a relatively large number of discretization lines to reduce numerical errors. This leads to larger matrices and longer computational time.

The higher-order approximation scheme of the second-derivative operator $\frac{\partial^2}{\partial x^2}$ presented in references [22, 42] gives sufficiently high accuracy and accurate estimation of the modal field profile and the effective indices. The necessary interface conditions for the electric and magnetic fields are appropriately included in the scheme. This scheme results in a much reduced matrix size, faster computational speed and lower memory usage. Derivation of five-point and seven-point approximation is presented in [22]. I have successfully programed the five-point and seven-point approximation of the second derivative operator ($\frac{\partial^2}{\partial x^2}$) to model a high contrast waveguide. The effective index n_{eff} and modal field of the fundamental TE and TM modes are calculated using the MOL. These MOL results are compared with exact results and their convergence behavior is studied by decreasing the mesh size (that is increasing the number of discretization points) in the problem space. It is observed that the 7-point formula gives a better estimate of n_{eff} and modal field with relatively few

sample points as compared to the 5-point and the 3-point formulas.

3.4.1 Air/GaAs/Air Symmetrical Waveguide

The waveguide structure considered is given in the inset of figure 3.3. In this simulation, a uniform mesh is used and number of sample points are varied while keeping the outer layer thickness sufficiently large so that the modal field decays to a sufficiently small value (approximately 10^{-5}) as compared to its value at the $Air/GaAs$ interface. The phase parameter, defined as $B = (n_{eff}^2 - 1^2)/(3.6^2 - 1^2)$. The exact values of the TE_0 and TM_0 modes are calculated by STF1 program (see Appendix **??**). For the TE_0 mode, we have $n_{eff} = 3.543961609340$ and $B_0 = 0.9665270809765686$, and for the TM_0 mode, $n_{eff} = 3.529434420038923$ and $B_0 = 0.9579353950966126$. The relative error in the phase parameter which is defined as $\frac{B_{MOL} - B_0}{B_0}$ is plotted against the mesh size (h) (see figures 3.3 and 3.4). The results show that for relatively small values of the mesh size, the error due to lower order formulation substantially exceeds the corresponding error for the higher order formulation. This shows the superiority of the 5-point and the 7-point formulation to find n_{eff} and modal field for both the TE and TM polarization as compared to the 3-point formulation.

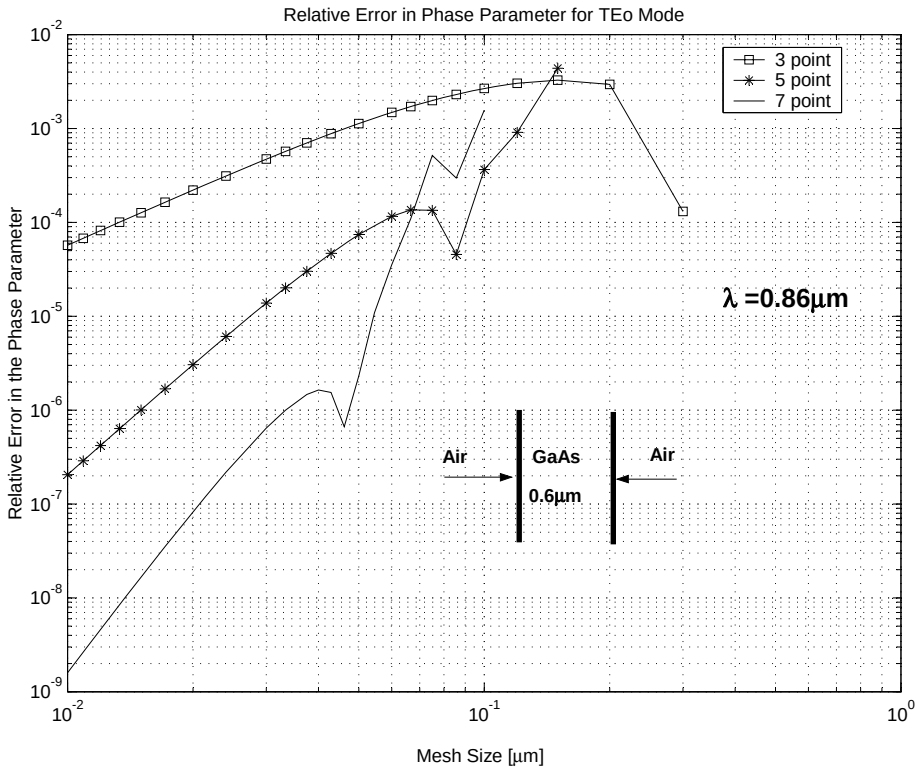

Figure 3.3: Relative Error in Phase Parameter for the fundamental TE_0 mode

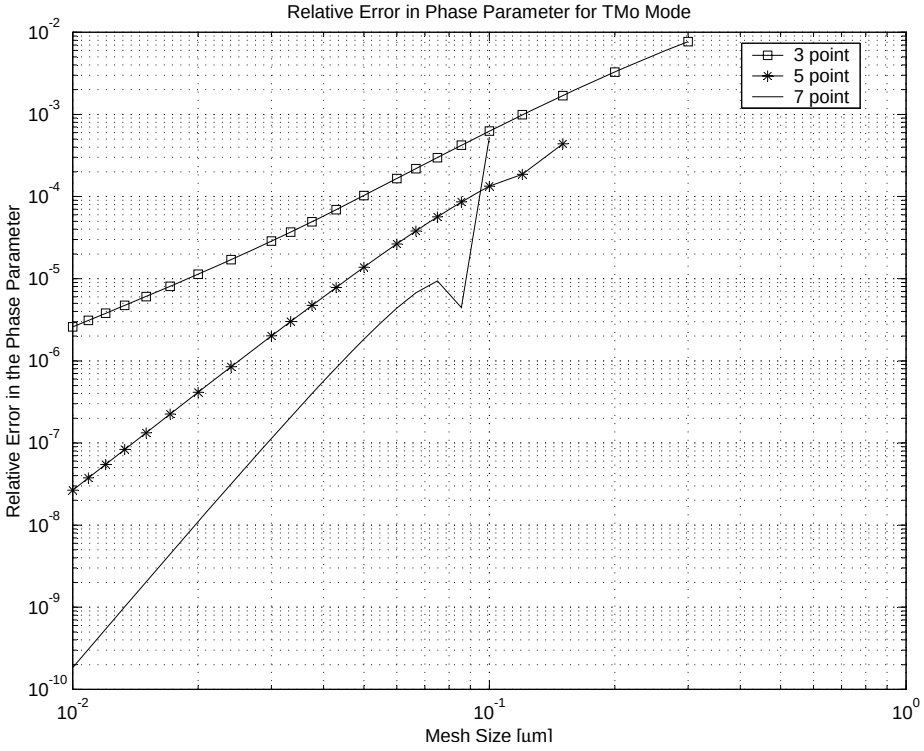

Figure 3.4: Relative Error in Phase Parameter for the fundamental TM_0 mode

Chapter 4

Analysis of Anti-Resonant Reflecting Optical Waveguide (ARROW) Modes

4.1 Introduction

Most optical waveguides, confine light inside the core, where the refractive index is higher than surrounding region, the cladding. There is a class of waveguides where the core refractive index is less than that of the cladding, these waveguides are well known as leaky waveguides and have found prominent position in the literature [24, 43]. These waveguides have many unique properties which have been exploited for several applications, such as building waveguides on high-index substrate [5],

confining light in gaseous medium [43], and remote switching [44]. Transmission capabilities are limited by the leakage loss as these waveguides not support guided modes. By careful design this loss can be reduced, and the most feasible way of realizing low-loss leaky waveguides is to surround the core with high reflective antiresonant cladding.

The Anti-Resonance Reflecting Optical Waveguide ARROW, a leaky waveguide (see figure 4.1), utilises the high reflectivity of two interference cladding layers (antiresonant reflection) deposited on the high index substrate. ARROW waveguides have received much attention due to their attractive features such as low transmission loss, high polarization selectivity, compatibility with monomode optical fibers [3] due to the large core size and small refractive index mismatch. They can be easily integrated monolithically with electronics components as they use SiO_2/Si material system [4].

Unlike conventional waveguides that depend on total internal reflection (TIR) phenomenon for guidance of the optical field in a region of high refractive index surrounded by region of low refractive indecies, the ARROW structure partially depends on antiresonant reflection [7] for guidance in a medium of low refractive index bounded on one or both sides by a medium of high refractive index. Since TIR is not realized on both sides of the core in this situation, the ARROW structure is essentially a leaky waveguide [8] and thus results in a complex propagation constant. The radiation losses of the leaky waves are reduced by the high reflectivity

of an antiresonant cladding layer. A typical ARROW waveguide is shown in figure 4.1. The ARROW structure is characterized by the presence of a high index layer n_2 which provides the high reflectivity required to achieve low loss operation of the waveguide. It is also noted that TE modes of the ARROW waveguide are generally low loss while the TM modes have high loss [5, 6] since TM reflections are always lower by the same phenomenon which gives rise to the Brewster angle. The degree to which TM loss is higher than the TE loss depends upon the details of proximity of the propagation angle in the core relative to the Brewster angle [5]. This ARROW wave-guide also behaves as a TE-pass polarizer and a wavelength filter.

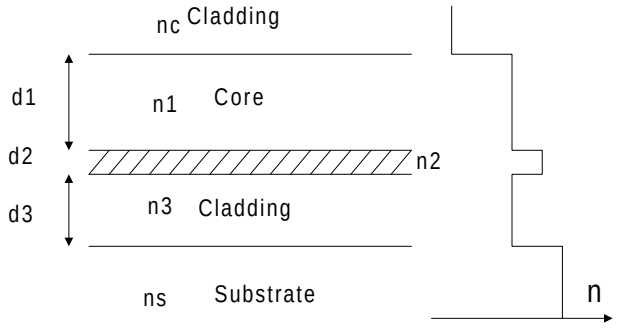

Figure 4.1: Typical refractive Index Profile in Planar ARROW Wave-guide

Because of its large mode diameter excellent coupling to external elements can be achieved, such as single-mode optical fibers. Moreover, the ARROW waveguides seem to be promising for integrating various electronic and topical devices on a sin-

gle semiconductor chip. In order to design integrated optical devices, it is necessary to know very precisely the propagation constant or effective index of the leaky modes of this structure.

M. A. Duguay and co-workers were first to propose the idea of ARROW [5]. The formulae to calculate the thickness of each layer are given in his paper. The modal characteristics of the ARROW waveguide are studied by many authors [45, 4, 46, 3]. In these papers, the ARROW waveguide is analyzed using equivalent transmission-line and transverse-resonance methods. In the previous work, much attention has been paid to the calculation of TE and TM mode losses of the ARROW Waveguide. In [8], the author describes loss calculation for ARROW waveguides using leaky mode solutions of the vector wave equation. General analytical expressions have been reported in the literature for TE, TM, HE and EH modes of multi-layer ARROW waveguides. In [4], standard-transfer matrix method is applied to ARROW waveguide and dispersion plots are given. The ARROW waveguides are also used in wavelength filtering. The structure itself is a wavelength selective structure as the anti-resonance condition is satisfied within a certain wavelength. So for wavelengths above or below the design wavelength, the modes will have higher loss. In [47, 48], the authors describe an ARROW-based optical wavelength filter. In [49], the design of an add/drop filter for wavelength division multiplexing is described. The filter is based on a directional coupler arrangement using two coupled ARROW waveguides.

4.2 Eigenmodes of a Basic ARROW

Basic ARROW structure is taken from references [5, 9] (see figure 4.2), but we calculated the width of the Buffer layer t_s = and high-index layer t_H (4.2) by the formula

$$t_m = \frac{\lambda}{4\sqrt{n_m^2 - n_{eff}^2}} \tag{4.1}$$

where t_m is the quarter wave thickness of the m-th layer ($m = s$ or H), λ is the free space wavelength, n_m is the refractive index of the m-th layer. We will choose the values of t_m such that anti-resonance occurs when the modal effective index, n_{eff} is approximately equal to the refractive index of the superstrate. At the operating wavelength $\lambda = 0.45\mu m$, using $n_{eff} = 1.333$ (which is equal to the refractive index of water) in equation 4.1 leads to $t_s = 0.189\mu m$ and $t_H = 0.060\mu m$ for $n_s = 1.46$ and $n_H = 2.3$ respectively. We will take a core size ($t_c = 4\mu m$). The Method of Lines is applied to model the ARROW structure of figure 4.2 and the results are compared with published as well as analytical results using ($STF1$). A close agreement is found between the MOL calculation of the effective index (real and imaginary parts) of the modal field with those available in the literature. A non-uniform mesh scheme is used in the MoL to model the device efficiently. A double layer PML is used as an absorbing boundary condition. It effectively absorbs the leaky field [45] [4] of the ARROW giving excellent open-space approximation. It is found during the simulation that the performance of the PML depends upon the mesh size and the

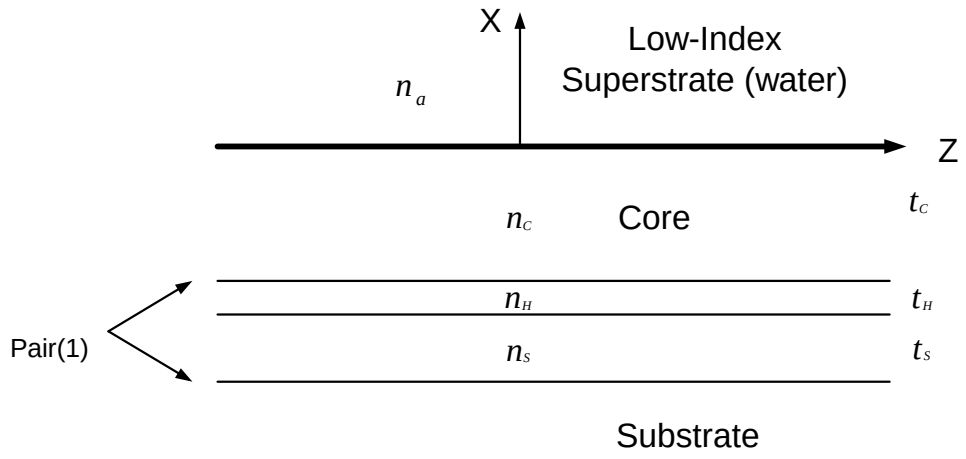

Figure 4.2: Basic Planar ARROW Wave-guide

total thickness of the PML. If the sampling period is large, the PML does not absorb the leaky modes effectively giving *reflections* of the leaky mode from the PML (standing waves pattern is observed). The same effect is observed if the PML thickness is small and if it is prematurely terminated by E/M wall. In this case, the modal field has not decayed to a sufficiently small value and reflection from the E/M wall occur. This reflection can make the calculated power loss much less than it actually is, so we must check for standing wave pattern immediately outside the PML and accordingly we must tune the PML by increasing or decreasing the mesh size. For correct results we must make sure that there is no standing wave pattern immediately outside the PML. To achieve this we must keep dense discretization lines in the first layer and a coarse mesh in the second layer to model a larger distance with relatively fewer sample points.

4.2.1 TE Modes

Figure 4.2 shows the basic ARROW strucure. The ARROW modes have complex effective indices (since they are leaky). The imaginary-part of the effective index is converted into power loss per unit length, that is in terms of dB/cm. The real part of the effective index lies between that of the cladding layer index and the guide layer index, that is $1.333 < {n_{eff}}' < 1.45$. The results for TE polarization are plotted in figures 4.3, 4.4, 4.5 and 4.6. The real-part of the effective index and power loss per unit distance are also given and found to be in close agreement with those in [5] and with analytical results (STF1). Note from Table 4.1 that only the lowest-order TE_0 mode has a small power loss of 0.64245 dB/cm, while all higher-order modes have much higher loss factor. On the other hand, all TM mode of ARROW are highly lossy. The high loss of the TM waves makes this device a single -mode waveguide and a TE-pass polarizer. All higher-order modes will decay significantly within a short propagation distance due to their high loss factor.

Mode	${n_{eff}}'$	Power Loss (MOL) (dB/cm)	Power loss (STF1) (dB/cm)
TE_0	1.4489691	0.64245	0.64633
TE_1	1.4458735	2.61797	2.629
TE_2	1.4407051	6.07767	6.084
TE_3	1.4334505	11.29668	11.259
TM_0	1.4489424	17.38	17.2996
TM_1	1.4457705	71.20	70.88
TM_2	1.4404865	167.06	166.28
TM_3	1.4330941	315.96	314.384

Table 4.1: Effective-Indices of different ARROW Modes

4.2.2 TM Modes

The simulations are repeated for the TM polarization and the results are shown in figures 4.7 4.8 and 4.9. The TM modes have much higher loss factor than the TE modes and they decay quickly within a shorter propagation distance.

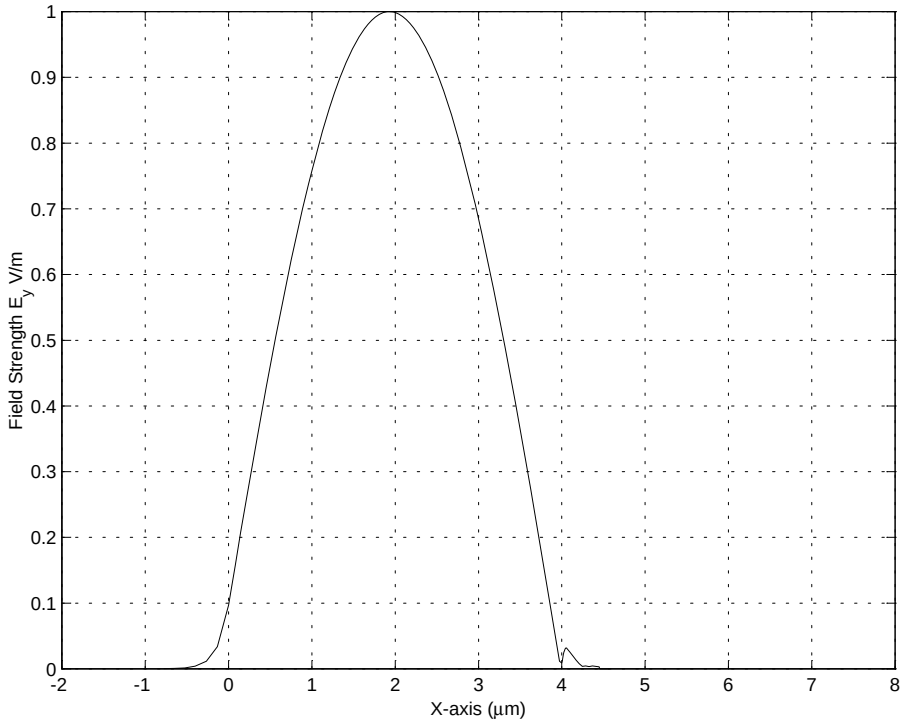

Figure 4.3: TE_0 Modal Field of the ARROW

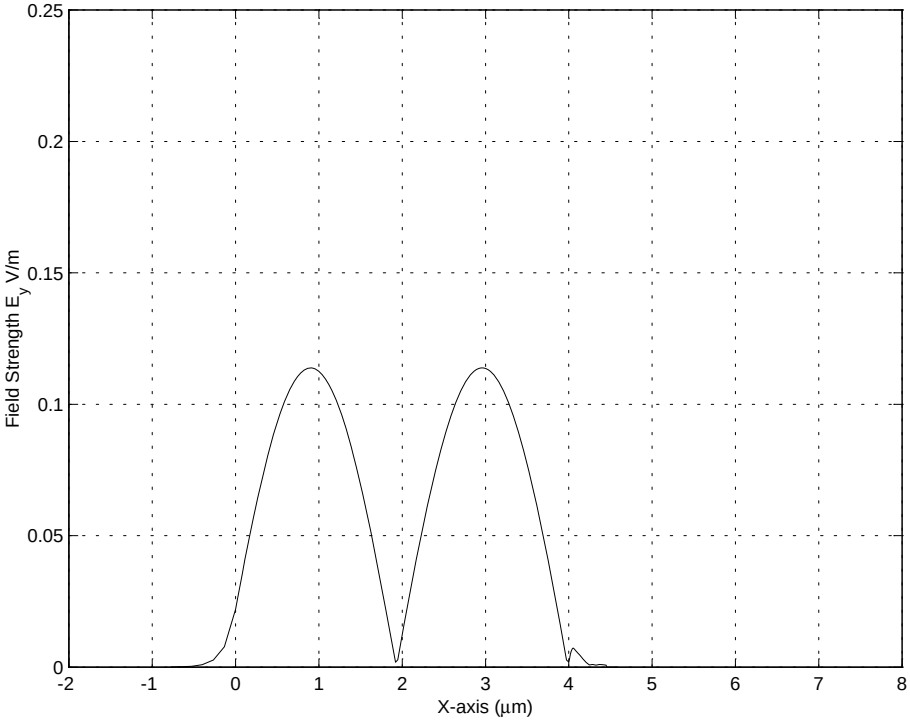

Figure 4.4: TE_1 Modal Field of the ARROW

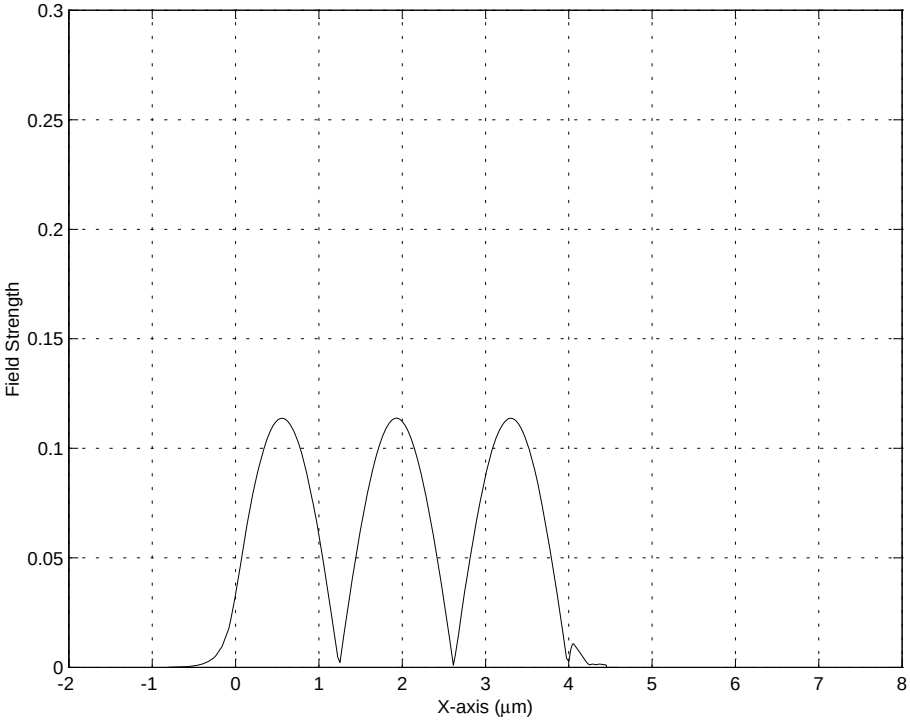

Figure 4.5: TE_2 Modal Field of the ARROW

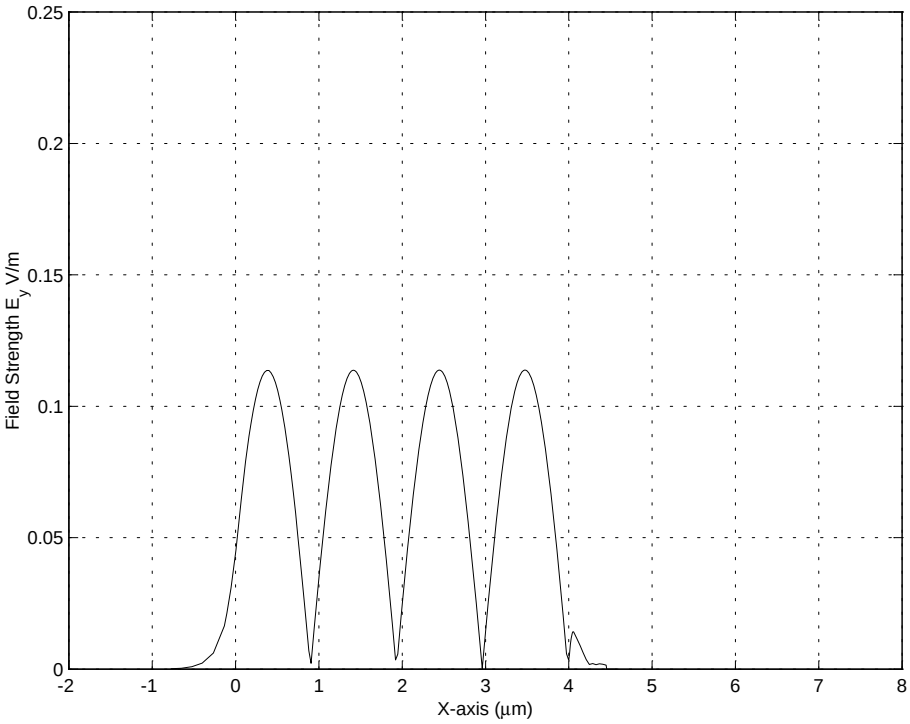

Figure 4.6: TE_3 Modal Field of the ARROW

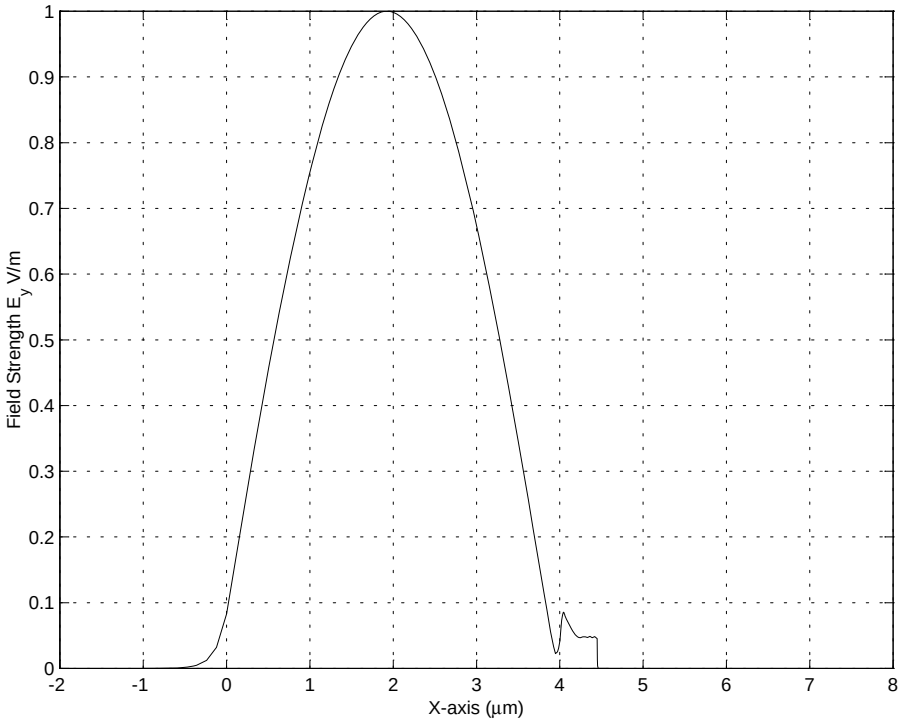

Figure 4.7: TM_0 Modal Field of the ARROW

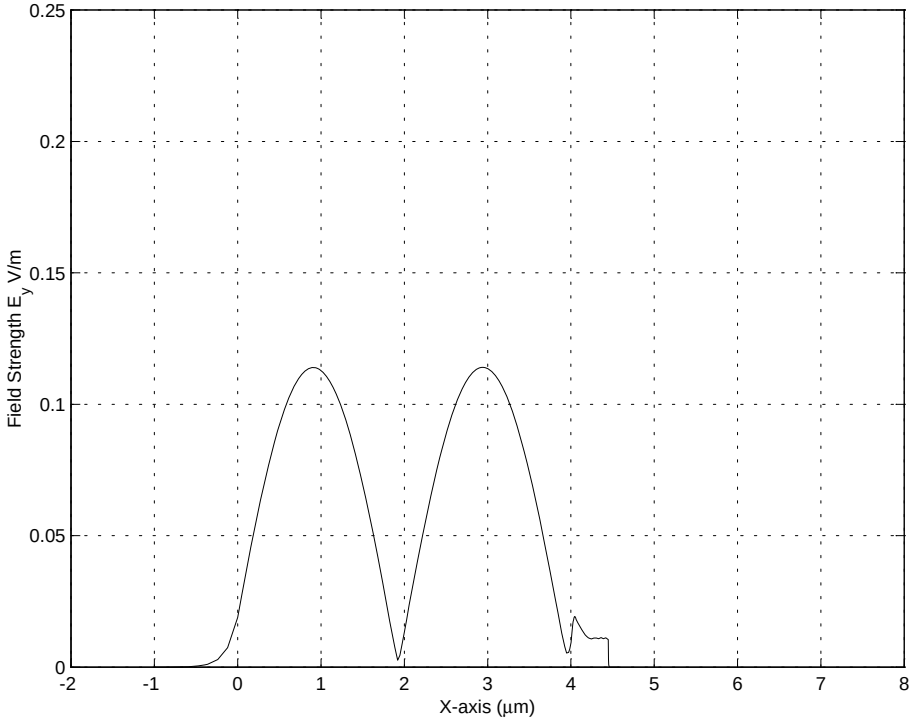

Figure 4.8: TM_1 Modal Field of the ARROW

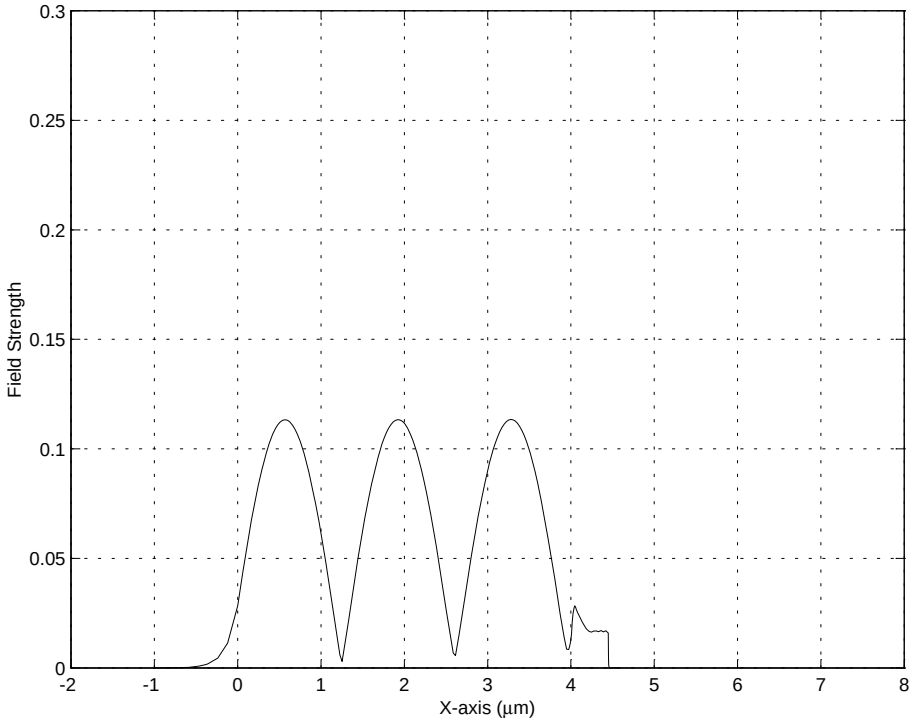

Figure 4.9: TM_2 Modal Field of the ARROW

Now we will consider the basic formulation and working of the PML layers.

4.3 Perfectly Matched Layer (PML) Absorber

Due to the discretization of $\frac{\partial^2}{\partial x^2}$, an electric or magnetic wall appears at the extreme edges of the computational window. This effect is not desirable, because the reflected field from the walls interferes with the field inside the computational window, leading to erroneous results.

The PML absorbing scheme based on the complex distance approach was first incorporated into the MOL by Al-Bader and Al-Jamid [23]. It has been shown in the literature that the PML can absorb propagating waves over a wide range of incident angles [23] resulting in a very small amount of reflected field. The absorption of the *radiative* wave is done by tranforming the distance x from the *real* domain to the *complex* domain. This results in an attenuation factor in the radiative field and hence causes decay of the radiative field in the PML region. The last mesh point is terminated by an electric/magnetic wall boundary condition. The *real* distance is transformed to a *complex* one according to:

$$x \rightarrow x(1 + j\sigma) \tag{4.2}$$

Here σ is the decay factor. The wave e^{+jkx} propagating in $+x$ direction in the real space will be transformed to

$$e^{+jkx(1+j\sigma)} = e^{+jkx}e^{-k\sigma x} \tag{4.3}$$

in the complex space. The factor $e^{-k\sigma x}$ results in the decay of the field in the $+x$ direction. The choice of the decay factor σ is discussed in [50]. Figure 4.10 shows

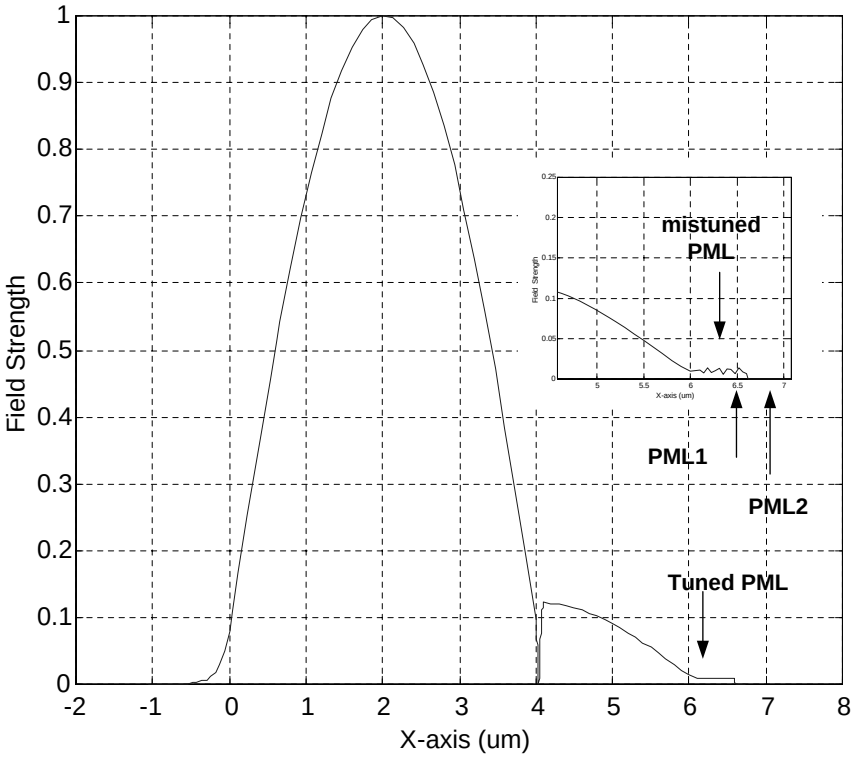

Figure 4.10: TM_0 Modal Field of the ARROW with tuned and Mis-tuned PML

the field due to a tuned and mistuned PML. If the PML is not properly tuned (has

an incorrect choice of parameters) then we observe standing wave pattern due to reflection from PML layers. If the PML is tuned properly then the standing wave pattern will die off immediately outside PML region and this indicates that our results, that is power loss and n_{eff} of the waveguide are computed correctly.

4.3.1 Miscellaneous results

Some Miscellaneous facts about the ARROW waveguide are observed which are documented. It has been observed that if the guide layer thickness is decreased while keeping all other parameters constant, the power loss of the fundamental ARROW TE mode increases. We also observed that if the ARROW layer thickness is varied from optimized value the waveguide becomes more lossy and the ARROW does not work in anti-resonance mode to suppress the radiation into the substrate, rather, it works in resonance mode and increases the leakage into the substrate. As the guide layer refractive index is made smaller, the peak of TE_0 moves towards the superstrate and the evanescent field is enhanced in the superstrate, this is accompanied by an increase in the leakage loss. If the guide layer refractive index is increased the field will be more confined to the core and leakage loss decreases. As a matter of fact, if layer refractive index is made higher than the substrate layer, and in this case the ARROW will behave as a regular waveguide with a TIR confined mode.

Chapter 5

Analysis of Multi-Layer ARROW Planar Waveguide

5.1 Introduction

Figure 5.1 shows the multi-layer ARROW. In this work we choose water as the low index superstrate material. The layer immediately below water is made of silica with an assumed refractive index $n_c = 1.45$ and thickness t_c. We shall refer to this layer as the core. The layer below the core is made of a high index material ($n_H = 2.3$) having thickness t_H. This is an ARROW layer [9] which is used here to cause wave reflection in the vertical direction towards the core layer. The next set of layers consists of a total of N identical pairs of layers. Each pair consists of a silica layer ($n_s = 1.45$) on the top of a high -index ($n_H = 2.3$) ARROW layer. The thickness

of the silica and the high-index layers are t_s and t_H respectively. The bottom most layer is the substrate, which is also assumed to be made of silica. When N=0, the total number of layers is exactly four(Basic ARROW see figure 4.2) . This includes the superstrate, the core layer, a single high-index ARROW layer and finally the substrate. We have used the same values of t_H and t_s and operating wavelength λ, mentioned in last chapter.

5.1.1 Multi-layer ARROW as polarizer

In last chapter (refer to figure 4.2, we have used only one pair of high and low index layers with a large core size $4\mu m$ to analyze the modes of the basic ARROW. We have chosen a large core size in order to reduce the leakage loss since extremely large leakage loss occur when the core size t_c is made small. Thus, a single layer of ARROW is unable to reduce the leakage loss to acceptable level when core size is small. However, as shown in figure 5.1and 5.2 that as N, the number of pairs increased, the leakage loss of the TE_0 mode is is reduced and becomes very small (below $0.1dB/cm$), when N=5 for all values of t_c.

Because the leakage loss of the TE_0 mode is sufficiently low for N=5 layers, we choose to fix the number of pairs used to N=5, before me make any further analysis. From figure 5.2 and 5.3, for N=5 layers the TE_0 loss is less then $0.1dB/cm$ and for the TM_0 loss is around $10^5 dB/cm$. As all TM modes are highly lossy, our proposed structure behaves as TE pass polarizer. In fact it passes TE_0 mode with low leakage

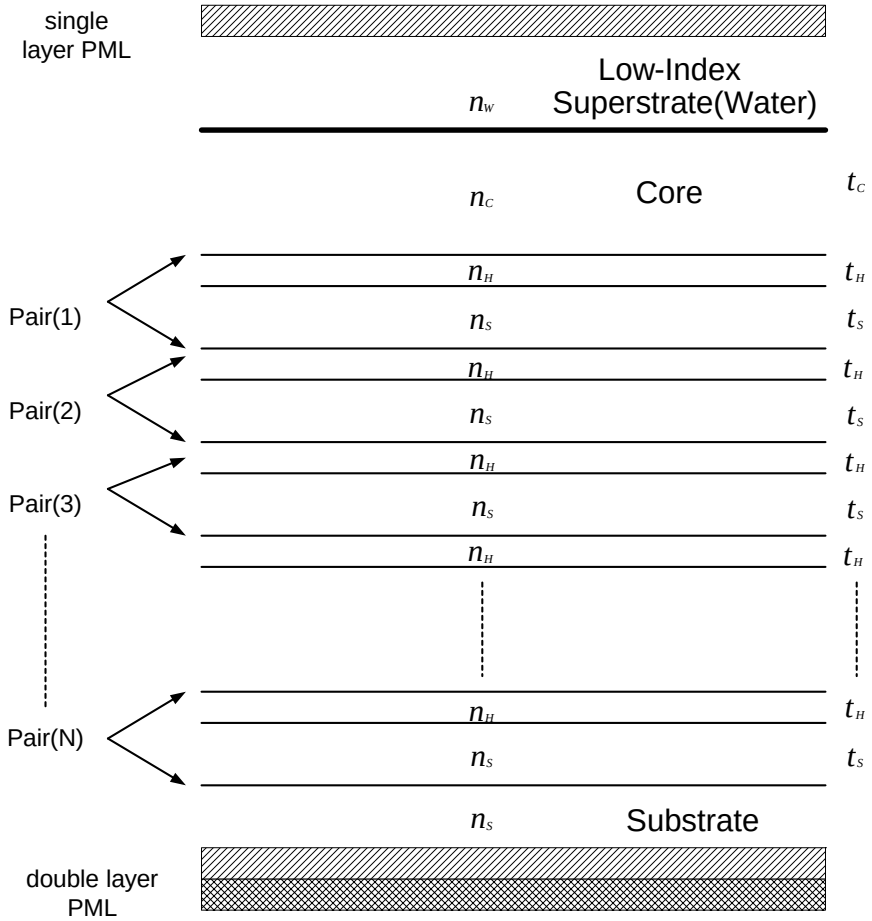

Figure 5.1: Multi-Layer Planar ARROW structure

loss as compared to higher modes. We can conclude that our proposed structure as single mode TE pass polarizer.

Before we proceed with other analysis, we must know some facts about the proposed structure. As seen from figure 5.2 and 5.3, the smallest core thickness is $0.2051\mu m$, if we decrease the core thickness below that value the N_{eff}, of the waveguide becomes less then 1.333 (i.e., below the refractive index of the superstrate). This corresponds

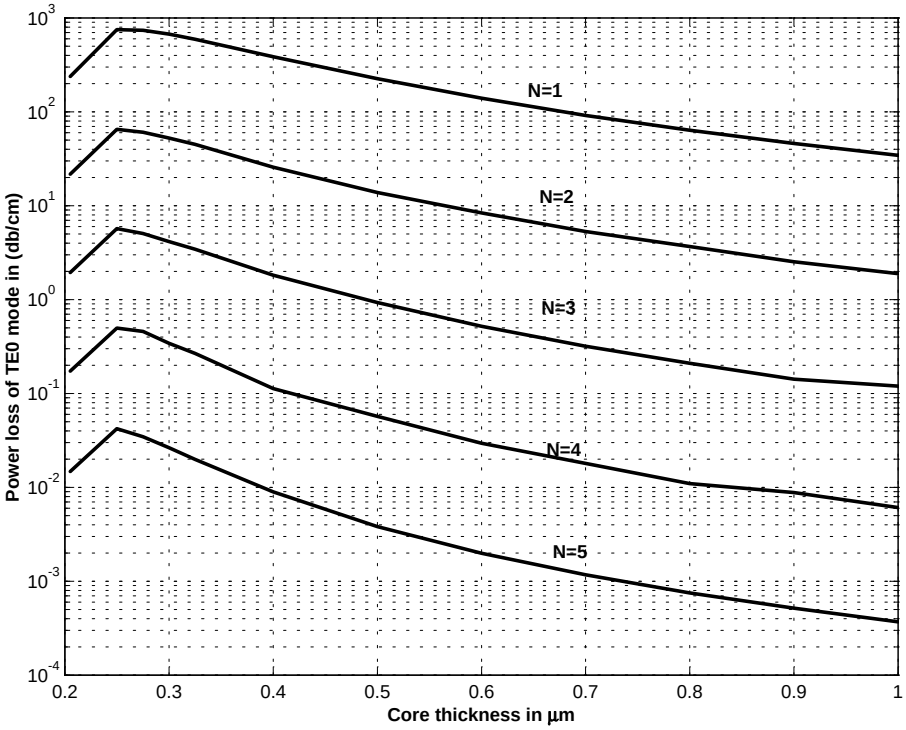

Figure 5.2: Variation of leakage loss of the fundamental TE_0 mode

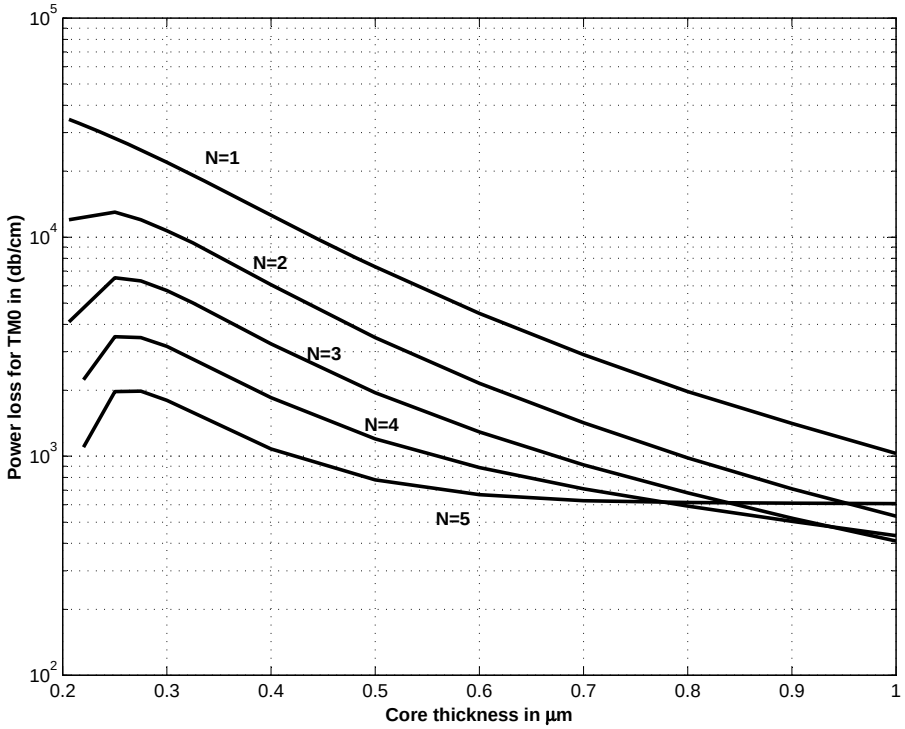

Figure 5.3: Variation of leakage loss of the fundamental TM_0 mode

to the cutoff of the TE_0. We have to look for the minimum core thickness (i.e. the cutoff core thickness) by trial and error procedure. This procedure is quite time consuming as we have to take care of reflection from the PML layers (there should be no ripples in PML region), mesh size for all pairs of layers and for all core thicknesses from $1\mu m$ to $0.2051\mu m$. We have checked all the results with the STF1 and we got 5 digits approximations for the power loss as well as for the real part of n_{eff}. It has been observed that a single discretization line and small variation of the width ($0.01\mu m$) in the PML region can alter the result significantly, so we should be careful in choosing the number of discretization lines in all PML regions as we change the core size.

5.1.2 Evanescent Field Enhancement in Low-Index Superstrate

A number of sensing methods for low-index materials are based on the use of the evanescent field of guided electromagnetic waves. The measured parameters include the refractive index variation [51], variation of material absorption [52] and detecting material flourescence [53]. The sensitivity of these methods is in general relatively poor. This is due to he fact that most of the guided optical power resides within the high-index waveguide core and substrate thus becoming inaccessible directly to the sensing process. In these cases only the evanescent part of the wave in the low index

superstrate and within a small distance (typically a fraction of wavelength) above the core is directly accessible for measurement. This part of the field carries only a small fraction of the guided wave power, a fact underlying the poor sensitivity of the measurements.

The main purpose of the proposed structure is the enhancement of the evanescent field in the low-index superstrate while maintaining low leakage loss. We assume that some measurement will take place in the low-index superstrate within a small distance (a few wavelengths) from the waveguide surface. For instance an absorption or phase delay measurement may be required in the low-index superstrate. Another possible measurement is the detection of material flourescence. The low-index superstrate may be air, any other gas or a low index fluid such as water.

Evanescent field enhancement in low-index superstrate is studied by many researchers for different sensing applications [54, 52, 55, 9, 56, 53], which we will see in detail in the next chapter.

Figure 5.4 shows the fundamental TE mode pattern of the multi-layer Arrow. It is clear from the figure that as the core thickness t_c is made smaller, the filed pattern shifts towards the water superstrate, instead of towards the substrate, which would be the case in conventional waveguides or in the case of a single layer ARROW waveguide. For $t_c = 0.81\mu m$, the electromagnetic field lies mostly in the core, however for $t_c = 0.21\mu m$, the field is compelled to move towards the water superstrate due to the high reflectivity from the stack of ARROW layers below the core [9].

This leads to the enhancement of the evanescent field in water. The interesting fact to note is that the peak of the field pattern remains in the core very close to the core-water interface for $t_c = 0.21\mu m$ and real part of n_{eff} approaches the refractive index of water ($n_w = 1.333$).

Figure 5.5 shows the fraction of the fundamental TE power in the superstrate and variation of the real part ($n_{eff}{}'$) of n_{eff} with respect to core thickness. It is observed that as t_c decreases, n_{eff} decreases and tends towards the superstrate refracative index (1.333). On the other hand the fraction of the power ($\zeta = \frac{\text{Power in superstrate}}{\text{Total power in the fundamental mode}}$) increases and tend towards unity. The value of ζ is 0.037 and 0.93 corresponding to $t_c = 1\mu m$ and $t_c = 0.2051\mu m$, respectively. As we can see there is an increase in the value of ζ by approximately a factor of 25 times. In calculating these results could not be automate the procedure, we had to take manual readings at all core thicknesses by adjusting the parameters discussed in previous section.

5.1.3 Sensitivity of the Multi-layer ARROW

Next we will show the effect of the field enhancement, we increase the refractive index of the water beyond 1.333 (i.e 1.334, 1.335 etc) and calculate the phase difference acquired by the fundamental TE mode. The phase difference (degrees/Millimeter)

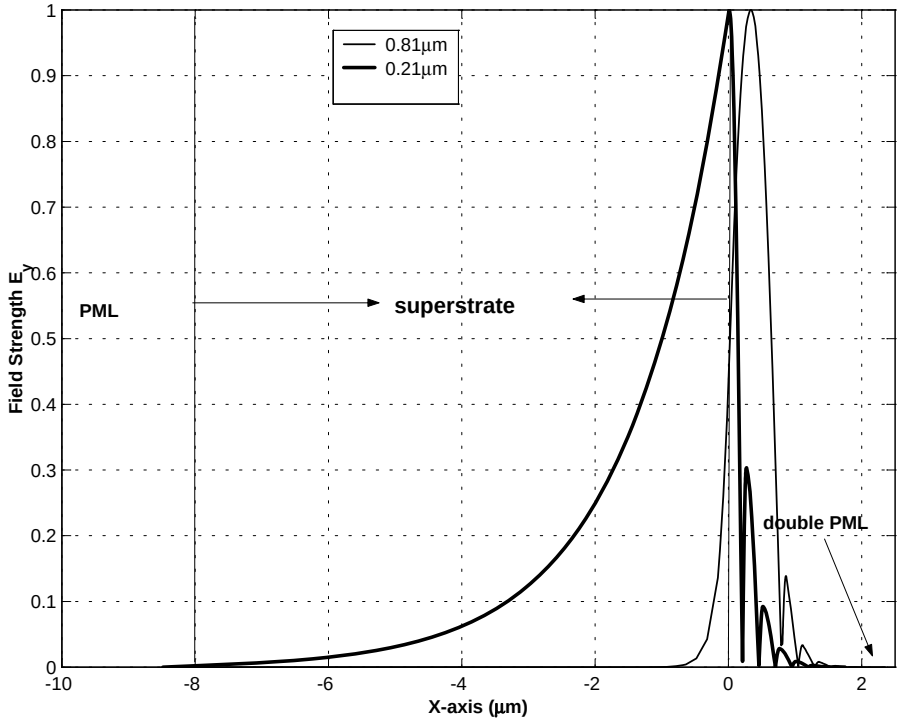

Figure 5.4: The Field Pattern of the TE_0 mode for two core thicknesses

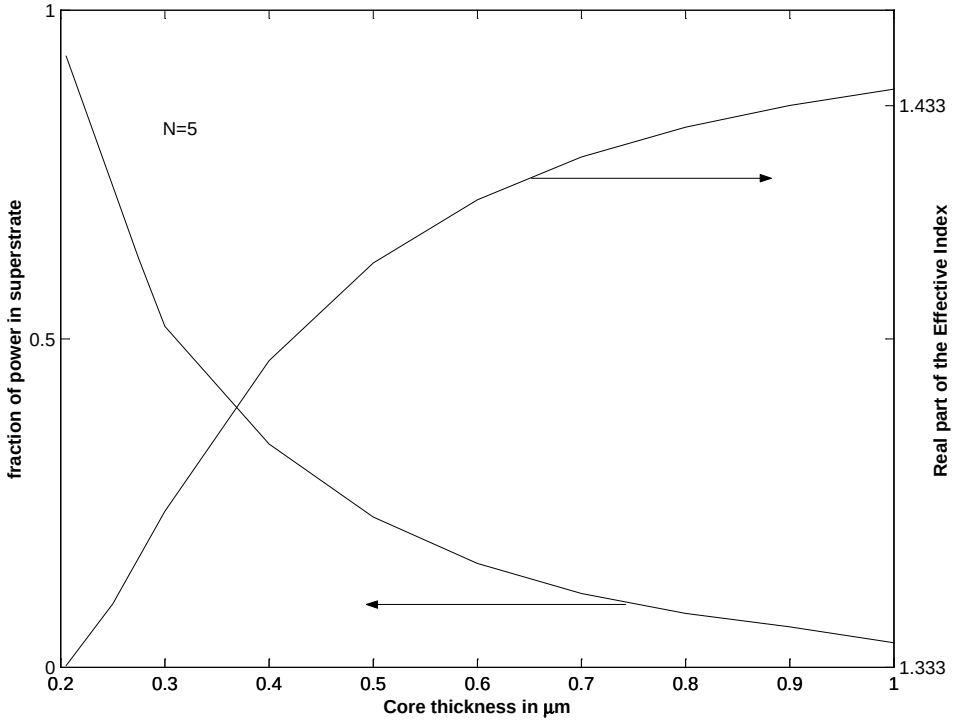

Figure 5.5: Fraction of Fundamental TE power in superstrate and Variation of the real part of the model effective index versus Core thickness

can be calculated by the formula:

$$\Delta\Phi = \frac{2\pi}{\lambda}\Delta n_{eff}\frac{180}{\pi}(1mm) \tag{5.1}$$

Where Δn_{eff} is the difference between two consecutive refractive indices. We have taken zero phase difference for the refractive index of water and used equation 5.1, for other phase difference calculations.

Figure 5.6 shows the acquired phase difference as a function of superstrate refractive index for $t_c = 0.21\mu m$ and $t_c = 0.81\mu m$. We can observe from the results that the acquired phase difference for $t_c = 0.21\mu m$ is approximately 20 times that for $t_c = 0.81\mu m$. The fact of significance is that an increase of 0.0004 in the refractive index of the superstrate, when $t_c = 0.21\mu m$, results in a phase difference slightly larger than 180 degrees per millimeter. This very high sensitivity may be required for some applications. We can always control the phase sensitivity by adjusting the value of t_c.

Figure 5.7 shows the variation of Modal loss as a function of bulk loss.

we define sensitivity as:

$$\chi = \frac{\mathrm{M}odalLoss}{\mathrm{S}uperstrateBulkLoss} \tag{5.2}$$

Bulk loss means the absorption loss introduced in the superstrate as seen by a plane

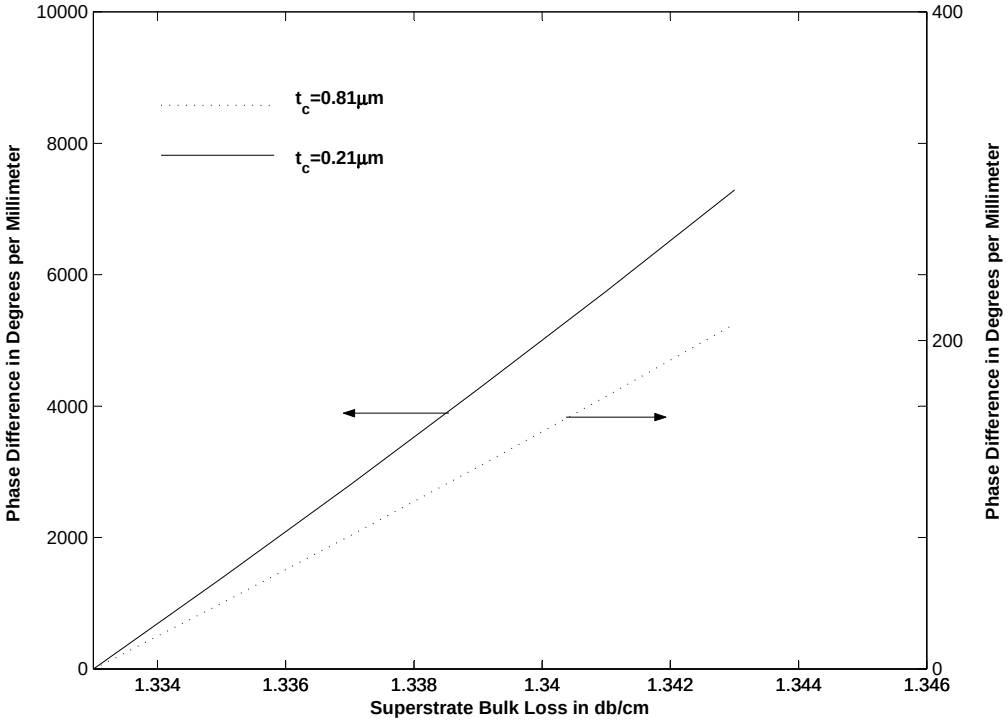

Figure 5.6: Acquired Phase Difference of the Fundamental TE -like mode as Function of Superstrate Refractive Index

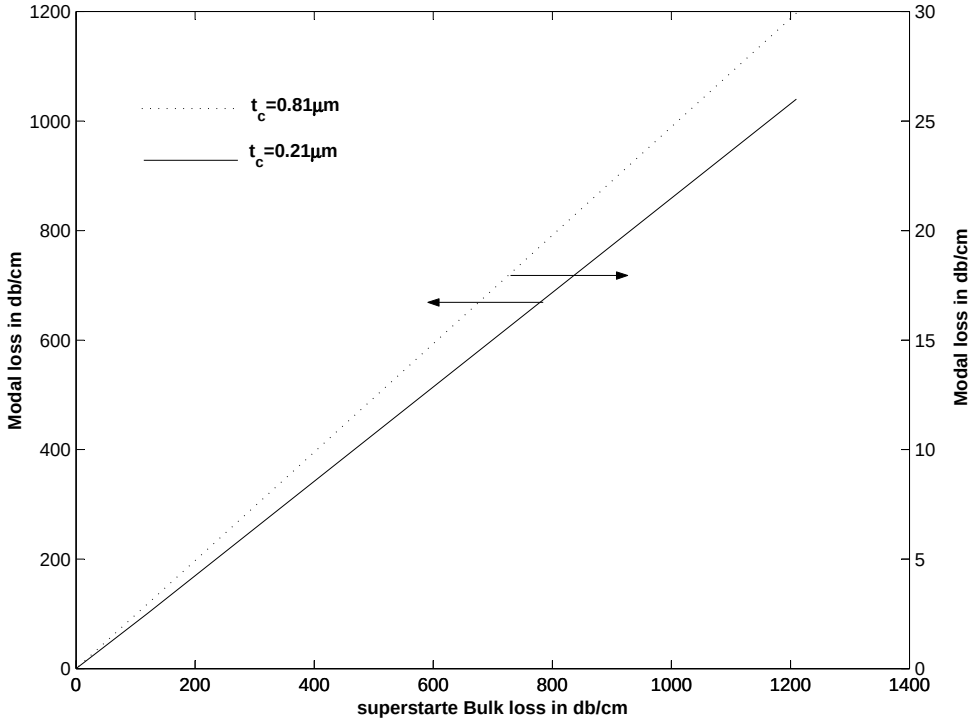

Figure 5.7: Variation of Modal loss of the Fundamental TE as a Function of Superstrate Bulk Loss

wave. This loss is represented as $n_s = 1.333 + j * 10^x$ where x we vary from -4 to -10.

It is clear from the figure that χ, is slightly less then unity for every point on the figure 5.7 for $t_c = 0.21\mu m$. It is interesting to note that for $t_c = 0.21\mu m$ sensitivity is approximately 35 times that for $t_c = 0.81\mu m$, which can be used to detect very small changes in refractive index, material absorption and material florescence.

Chapter 6

Application of Evanescent Field Enhancement in Low-Index Superstrate

6.1 Introduction

The main purpose of this chapter is to study the applications of the evanescent field enhancement in low-index superstrate. All applications can be broadly classified under three headings.

- Chemical Sensing
- Biochemical Sensing

- Biosensing

Optical sensors detect changes in the properties of light in the ultraviolet, visible, and infrared range, which are caused by an interaction between electromagnetic waves and matter. The different measuring optical parameters are: absorbance, fluorescence (intensity, decay, polarization,energy transfere), bio-and chemiluminescence, phosphorescence, thermoluminescence, light scattering, evanescence, surface plasmon resonance(SPR), refractive index, total internal reflection (TIR), and interferometry. For detailed discussion refer to reference [57].

Optical sensors may be subdivided as

- Sensors that measure direct optical quality : absorbance, fluorescence, luminescence etc.

- Indicator-sensors, where an optically active indicator ($pH-, O_2-, H_2O_2$-sensitive dye)is immobolized at the tip. For example oxygen is known as a quencher of the fluorescence of aromatic compounds. These sensors are used to quantify nonoptically active analytes such as oxygen, carbondioxide and protons.

- Bio-sensors, sensors where biorecognition elements is co-immobilized to an indicator-sensor. The biorecognition element mediates between the analytes and the transducer/detector.

Conventional high-index waveguides usually rely on the presence of an evanescent field in the low-index superstrate to sense the surface refractive index, optical absorp-

tion or fluorescence associated with the sensing reaction. To maximise sensitivity, the high index waveguide is normally made as thin as possible while maintaining the low-loss guidance of at least one guided mode, thus maximising the intensity of the evanescent field. ARROWs can be used to confine the light in a low index layer, such as water, providing much higher sensitivity than a conventional waveguide, as virtually all light propagates in the low index layer.

Chemical sensing and biosensing can take place within low-index layers compatible with ARROW operation. Chemical sensing was performed using low-index polymer layers to detect low molecular weight hydrocarbons in air and water, while biosensing can be done using antibodies covalently coupled to dextran gels.

There is great demand for sensors that can translate the concentration of various chemical compounds to the electrical domain. These sensors are for example required in process control, environmental monitoring, health care, biotechnology and the automotive industry. In some applications it is advantageous to use optical domain as an intermediate between the chemical and electrical domain. The reasons for this can be

- the absence of electromagnetic interference
- no danger for explosions due to the passage of electrical currents.
- high sensitivity to many measurands
- specific optical sensing mechanisms, such as chemical analysis by means of

material specific absorption wavelengths

Many characteristics of light are available to carry the sensor information. For example the phase, the intensity (distribution), the direction of propagation, the polarization or the wavelength can be used. In many situations it is preferred to incorporate optical sensors in a waveguide system, either fiber or integrated optics based. Compared to the use of free space beams this guided wave approach offers the potential advantages of:

- a better control of the light path, with no alignment of the experimental setup required
- use of thin chemo-optical interface is possible because of the evanescent field, which permits large interaction length.
- remote sensing is possible by the use of a fiber.
- a higher mechanical stability
- reduced weight, size and price

Fiber based sensors compared to integrated optics are very cheap and have the strong advantage that they can be easily applied for distributed sensing. The sensor can be incorporated in the fiber that transports the light from the source to the detector and the different sensors can be read out in, for example, the time domain

(OTDR) or wavelength domain (in case Bragg-reflectors are used). Nevertheless, fiber sensors cannot compete with integrated optics with respect to:

- robustness
- compact optical circuitry, enabling a higher complexity (e.g. multiple sensors on one chip)
- design flexibility with respect to the geometry as well as the choice and combination of materials (for example active and passive materials)
- ease of access to the optical path in evanescent-field sensing
- potential of integration with micro-electronics, micro-mechanics and micro total analysis systems (μ TAS)
- potential of cheap batch-wise mass production
- benefits from the developments in guided wave devices and microsystems in optical telecommunication

The degree of integration of a sensing scheme depends entirely on the intended application. Selection criteria will for example arise from the required sensitivity, selectivity, sensing environment, size or cost price. From literature, on one hand very sensitive sensing systems are known where only the sensing element is a planar waveguide and where the light from a bulk laser is coupled into and out off the

waveguide by means of prism, grating or end-fire coupling. This type of devices will be very suitable for applications in e.g. medical laboratories. On the other hand, channel waveguide based sensors where the source, a phase modulator and a detector are monolithically integrated on the chip have been reported. Due to their small size and weight these sensors might be especially suitable for applications in e.g. space or micro TAS. These two examples illustrate that there is no ultimate choice for using end-fire, butt-end, grating, prism, hybrid or monolithically-coupled light sources or detectors, for the use of channel or slab waveguides, or for on or off-chip modulation, referencing and signal processing. Every sensing problem requires for a different solution.

In our thesis we focus on evanescent field sensing application in many areas. There are many types of sensors which can utilize evanescent field. Our aim here is to enhance the evanescent field in the low-index superstrate and study the effect of the enhancement on the sensitivity of the optical devices used. Many types of chemical and biochemical sensors are reported in the literature which are based on absorptiometry or refractiometry of evanescent waves in the integrated optics waveguide. Chemical and biochemical sensors are key elements for the following applications, including (1) Medical engineering, (2) Biochemical engineering, (3) Environmental engineering, (4) Factory auto-processing (5) gas,petroleum and ground water monitoring, (6) Alarm system, (7) Sensors in automobiles,(8) consumer products. With micro-electro-mechanical techniques developed recently, optical sensors can be

miniaturized and integrated with fiber optics communication WDM systems to form a multi-processing sensing systems.

6.2 Chemical and biochemical sensors

Waveguide chemical sensors find use in a wide range of applications such as detection of harmful gases (Methane,$Co2$,$So2$), [52, 58, 51]monitoring pollutants and other compounds in water, pH (hyderogen ion concentration) detection, and in the broad field of immunological assays (Laboratory tests are carried out by hospitals to determine the concentration of particular chemicals and biochemicals in blood samples, in order to diagnose disease states and to monitor therapy. A significant, and fast growing, part of this market is immunological assay often shortened to immunoassay), detecting the concentration of certain chemicals in blood, monitoring glucose concentration.

The sensing of chemical parameters is usually performed by monitoring changes in a suitably selected optical property. Depending on the particular device, the optical property measured may be absorbance, reflectance, scattering (due to turbidity), or luminescense (fluorescence or phosphorescence).

In chemical sensing, an analyte (the material to be measured) is placed in the evanescent field of the wave-guide. Change is observed in the absorption or phase shift of the light propagating through the waveguide, giving an indication of the concentra-

tion or refractive index of the analyte. In the case of sensors based on phase shift, the measured difference in phase between the analyte and a reference material can be used to determine the change in effective index, $neff = \beta/k_0$, of a particular optical waveguide mode. The change in phase caused by the analyte can be precisely monitored with a Mach-Zehnder interferometer [51].

Luminescense is a very important optical property used for chemical sensing. Measurement of luminescense (usually called either fluorescence or phosphorescence depending on the the fluorescent lifetime) is an extremely sensitive technique, capable of measuring low analyte concentration.It is particularly well suited as both exciting light(evanescent field) and the fluorescent light have wavelength, significantly different. There is often several tens of nm difference in optical wavelength between source and fluorescent light.

The technique used for fluorescence is to prepare a coating of fluorophore(fluorescent indicator dye or fluoro reactand) on the upper surface of the waveguide core [59, 58]. Fluorophore is sensitive to the target analyte which means a change in fluorophore produces a change in the target analyte depending on the concentration of the target analyte. As the evanescent field propagtes, it stimulates fluorescence from the fluorophor. The intensity of fluorescence is dependent on concentration of the analyte. A portion of the fluorescence is then captured and travel down in the opposite direction of the initial pulse. The fluorescence can be measured (fluorimeter or spectrofluorimeter) and analyte concentration can then be determined. By monitoring

the time delay between the outgoing pulse and incoming fluorescence one can spatially map the analyte concentration along the sensor length.

Fluoroscence technique finds a wide range of application such as oxygen detection by quenching of fluoroscence (A fluorescent dye is absorbed on a polymeric substrate membrane, which is oxygen-preamble.Absorption of oxygen through the membrane reduces the fluorescent efficiency of the dye. which is termed fluorescent quenching) in an oxygen sensor for medical applications [59] measurement of physiological oxygen concentration is very important, particularly for patients with acute medical conditions undergoing major surgical procedures such as heart artery bypass and grafts. Two distinct measurement have to be made. In the first, the oxygen-carrying state of the blood is monitored by assessing the colour, and hence the oxygenation, of the hemogloben. The second measurement yields a value for the concentration (partial pressure: pO2, or oxygen tension) of oxygen gas dissolved in the blood stream. Research has been done to measure amines using fluoro reactands [58] and technique to measure molecular recognition of neutral analyte concentration is discussed. Numerous chemical species can be monitor such as sulphates, acitinides, inorginic chloride, hydrogen sulphide.

As sensors based on fluorescence mostly use changes in intensity as the analytical information, many fluororeactands performs reversible chemical reaction with the analyte, causing changes in luminescence intensity, this property can be used for analytes having different concentrations or multiple number of analytes concen-

tration can be determind simultaneously. Other chemical sensing applications of optic fluorimetry include such widespread aspects as detection of stomach cancer, the detection of coal tar contamination on the skin, mapping the distribution of algae (plankton) in lakes and detecting herbicide residue in plant leaves. Many of fluoroscence applications are in the medical field which will be discussed in next section.

Another optical property used in chemical sensors is absorption which is used to detect explosive gases such as methane [58] using a teachnique called gas spectroscopy. Light scattering is also an important measurement in many applications. Examples include the determination of impurities in liquids [58] and the measurement of particle size. One of the most commercially developed sensor yet developed is an oil-in-water monitor for measuring the oil pollution in effluent (sewage) water. Measurement of the extent of surface scattering from opaque surfaces has been done, for the determination of the degree of demineralization of tooth enamel, fat content in milk, and the whitness of the eyeball.

6.3 Biosensors

6.3.1 Introduction

Human kind has been performing bioanalysis since the early times, sensory nerve cells of the nose is used to detect scents, the enzymatic reactions in the tongue

to taste food. As the time is passed and also the level of understanding of the function of living organism in detecting traces of biochemicals in complex systems because biological organisms are some of the most efficient machines ever created and the recognition abilities of biological organisms for foreign substances is unparalleled, researchers have sought to apply and copy their efficiency for use in man made creations. Using bioreceptors from biological organisms or receptors that have been patterned after biological systems, scientists have developed a new means of chemical analysis that often has the selectivity of biological recognition systems. These biorecognition elements in combination with various transduction methods (ex:Optical transduction) have helped to create the rapidly expanding field of bioanalysis and related technologies known as bioreceptors and biochips.

For the last decade, biosensors had been revolutionised almost all fields of medical technology- significantly improving patient care and reducing overall operating costs, providing potentially billion-dollar markets for sensor manufacturers. Optical biosensors represent the second major family of biosensors (after electrochemical biosensors) to have been exploited commercially. This was possible by progress in fibre-optic technology, laser miniaturisation and the reproducible manufacture of prisms and waveguides. Some optical biosensors are best seen as miniaturised versions of "traditional" spectrophotometers, while others are based on new, integrated-optic methods such as evanescent waves [60] and light-addressable potentiometric semiconductors. However, due to persisting cost and size issues, mass markets are

not presently feasible-optical biosensors seem set to remain powerful research tools for the foreseeable future.

6.3.2 Biosensing Principle

A biosensor [61] can be generally defined as a device that consists of a biological recognition system, often called a bioreceptor, a transducer and an amplification/processing unit see figure 6.2. conventional techniques for transducer include: 1) optical measurements (i.e. luminescence, absorption, surface plasmon resonance, etc.) 2) electrochemical and 3) mass-sensitive measurements (i.e. surface acoustic wave, microbalance, etc.). The interaction of the analyte with the bioreceptor is designed to produce an effect (optical change) measured by the transducer, which converts the information into a measurable effect (through signal processing the interaction is converted into digital values that relates to the build-up of concentration or activity of the analyte in the vicinity of the device, which in turn relates to the ambient level in the bulk sample under inestigation). Biosensor can also be defined as an analytical device incorporating a deliberate and intimate combination of a specific biological element (that creates a recognition event) and a physical element (that transduces the recognition event. A biosensor is not only a stand alone entity, but should be considered as a part of a general development in instrumentation, designed to address generic medical and non-medical measurement science problems.

Conceptual principle of the biosensing is illustrated in figure 6.1 and 6.2. In figure 6.2 a permselective membrane is shown which is used with some devices to control transport of analyte to the biological recognition layer(enzyme, antibody, DNA) that generates a response on interaction with the analyte, leading to an electrical signal generated by the transducer [62]. Many optical biosensors represent miniaturised

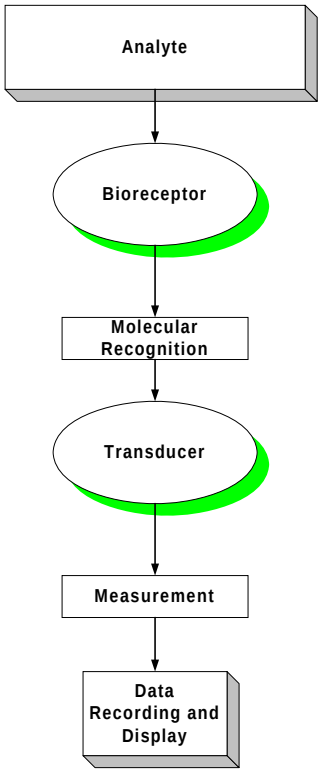

Figure 6.1: Conceptual diagram of the biosensing principle

versions of classic spectrophotometers; a means of generating light of a particular wavelength (or wavelength band), a means of channelling that light into the sample, and a means of measuring the intensity of light that passes through (or is scattered by) the sample. The most amenable element to miniaturisation is the light-guide

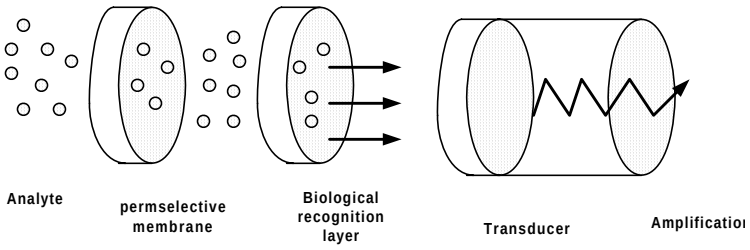

Figure 6.2: Schematic representation of a biosensor

the part in contact with the sample. The most exploited system of this type is a Planar waveguide, or fibre-optic cable, coated with a biological element. Light is introduced into the sample via the fibre or core of waveguide. Certain wavelength of incoming light is absorbed or alternatively scattered depending on the number and type of molecules present on the surface of the core.

The light that traverses (or alternatively that which is scattered back by) the biological layer is measured. The outgoing spectrum will be different from the incoming spectrum. This difference is measured, and when compared to a calibration or reference, allows determination of the level of analyte.

Of course, optical biosensors are just optical sensors where the recognition element is of biological origin. This gives greater specificity for the analyte, for example that given by binding of antigens (A foreign substance which, when introduced into body, stimulates the production of an antibody) to a layer of immobilised antibodies(These are proteins, produced by the immune system of higher animals in response to the entry of "foreign"(antigen) materials into the body-for example, viruses, bacteria

and implanted medical devices).

6.3.3 Bioreceptrors (Bioelement)

A bioreceptor [61] is a biological molecular species (e.g., an antibody, an enzyme, a protein, or a nucleic acid) or a living biological system (e.g., cells, tissue, or whole organisms) that utilizes a biochemical mechanism for recognition. Bioreceptors are the key to specificity for biosensor technologies. They bind the analyte of interest to the sensor for measurement. They can take many forms and different bioreceptors have been used are as numerous as the different analytes.

The sampling component of a biosensor contains a bio-sensitive layer. The layer can either contain bioreceptors or be made of bioreceptors covalently attached to the transducer. The most common forms of bioreceptors used in biosensing are based on 1) antibody/antigen interactions, 2) nucleic acid interactions, 3) enzymatic interactions, 4) cellular interactions (i.e. microorganisms, proteins) and 5) interactions using biomimetic materials (i.e., synthetic bioreceptors). To undeerstand the concept of sensing we will briefly discuss the five common bioreceptors.

Antibody/Antigen

An antibody is a complex biomolecule, made up of hundreds of individual amino acids arranged in a highly ordered sequence. They are biological molecules that exhibit very specific binding capabilities for specific structures. This is very important

due to the complex nature of most biological systems. For an immune response to be produced against a particular molecule, a certain molecular size and complexity are necessary: proteins with molecular weights greater than 5000 Da are generally immunogenic. The way in which an antigen and its antigen-specific antibody interact may be understood as analogous to a lock and key fit, by which specific geometrical configurations of a unique key enables it to open a lock. In the same way, an antigen-specific antibody fits its unique antigen in a highly specific manner. This unique property of antibodies is the key to their usefulness in immunosensors where only the specific analyte of interest, the antigen, fits into the antibody binding site.

Enzymes

Enzymes are large protein molecules that catalyse chemical reactions. In a simplified scheme, the enzyme participates actively in the transformation of a chemical A to chemical B but remains unchanged at the end of the reaction. In biosensors enzymes being used are very specific tools as enzymes are very specific in their action any given enzyme will always turn A into B and never C (if you want C from A, then there will be different enzyme dedicated for the purpose). So the specificity of enzymic action is the basis for the enzyme-based biosensors.

Nucleic acids

Deoxyribonucleic acid (DNA) or ribonucleic acid (RNA), constitutes another biorecognition mechanism which are the building blocks of genetics. In the last decade, nucleic acids have received increasing interest as bioreceptors for biosensor and biochip technologies [61]. The complementarity of adenine : thymine (A : T) and cytosine : guanosine (C : G) pairing in DNA, forms the basis for the specificity of biorecognition in DNA biosensors, often referred to as genosensors. If the sequence of bases composing a certain part of the DNA molecule is known, then the complementary sequence, often called a probe, can be synthesized and labeled with an optically detectable compound (e.g., a fluorescent label). By unwinding the double-stranded DNA into single strands, adding the probe, and then annealing the strands, the labeled probe will hybridize to its complementary sequence on the target molecule.

Cellular Structures/cells

Cellular structures and cells comprise a broad category of bioreceptors that have been used in the development of biosensors and biochips. These bioreceptors are either based on biorecognition by an entire cell/microorganism (Fungus, bacteria etc) or a specific cellular component that is capable of specific binding to certain species. There are presently three major subclasses of this category: 1) cellular systems, 2) enzymes and 3) non-enzymatic proteins.

Biomimetic receptors

A receptor that is fabricated and designed to mimic a bioreceptor is often termed a biomimetic receptor. To construct these receptors several different methods have been developed. These methods include: genetically engineered molecules, artificial membrane fabrication and molecular imprinting. The molecular imprinting technique, which has recently received great interest, consists of mixing analyte molecules with monomers and a large amount of crosslinkers. Following polymerization, the hard polymer is ground into a powder and the analyte molecules are extracted with organic solvents to remove them from the polymer network. As a result, the polymer has molecular holes or binding sites that are complementary to the selected analyte.

6.3.4 Labelled and non-Labelled Optical sensor

One can essentially distinguish two general types of optical sensor labelled and non-labelled optical methods. Any given chemical will have a unique "finger-print" spectrum when examined by most spectroscopic methods. The molecule of interest (i.e. the analyte) is not present alone in the sample but is part of a "soup". All these different molecules contribute their spectral features (in proportion to their concentrations) to the overall, measured spectrum of the sample. In a some cases, the spectrum of the desired analyte will be so different from those of its partners in

soup that it can be easily and directly identified and quantified. But in cases where this is not true, an artificial, optical labels must be added to the system.

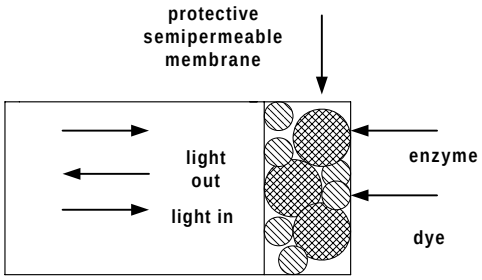

Figure 6.3: Labelled optical sensor1

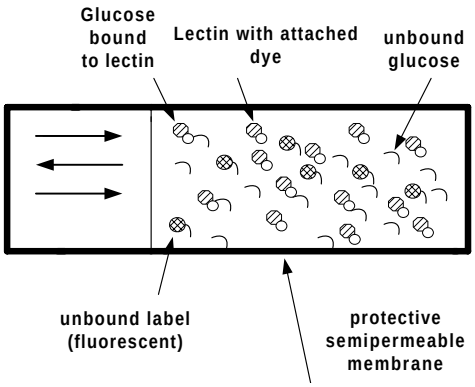

Figure 6.4: Labelled optical sensor2

We will discuss labelled and non-labelled sensing methods so we can be clear in our understand as we proceed further.

This is best explained by reference to the biosensors for glucose shown in figure 6.3 and 6.4. The reaction of glucose and oxygen with create some intrinsic optical effects, the change is not great and methods which produces greater change is developed. In figure 6.3, the device is composed of the transducer, a fibre optic cable,

and a sensing layer composed of a synthetic dye (the optical properties of which depend on its immediate environment) and the bioelement (which in this case is familiar glucose oxidase (GOD)) [63]. The breakdown of each molecule of glucose (catalysed by GOD) consumes oxygen (O2) and produces a proton (H+). The dye chosen would be one sensitive to the surrounding pH, or to the surrounding oxygen concentration. Thus, when the sensor is immersed in the sample, the spectrum of the dye recorded depends on, and thus gives, the glucose concentration (assuming that the pH and oxygen concentration have not changed non-specifically for any other reason.

In figure 6.3 an elegant but more sophisticated and complicated optical affinity biosensor for glucose is shown [64]. The bioelement/recognition layer is a lectin, a type of protein that specifically binds sugars. The mere binding of glucose to lectin does not significantly change the optical characteristics of the respective molecules, and so cannot be detected directly. so the solution is an indirect estimation of glucose binding by following the behaviour of a artificial "label" molecule which competes with native glucose for the available lectin sites. Thus the sensing principle is based on measuring how much label is bound to lectin, and how much is unbound the more glucose is present, the more label will be displaced. The label itself is a sugar molecule with an attached fluorescein group (fluorescein is a fluorescent molecule it absorbs light energy of a particular wavelength and then rapidly emits that energy, but as light of a longer wavelength, i.e. of a different colour). This in turn means

that one needs to distinguish bound from free labels. This is cleverly achieved by additionally attaching a dye molecule (rhodamine) to the lectin. When the label is free in solution, i.e. after being displaced from lectin by glucose, it fluoresces normally. However, when bound to the lectin, the fluorescein-labelled glucose still adsorbs light energy, but instead of emitting, transfers it to the rhodamine the fluorescence is "quenched".

It must be borne in mind that the labelled sugar may not bind to lectin with the same affinity as does native glucose; the binding may be stronger or weaker. This may or may not be a problem: if the binding of the label is stronger, proportionally more glucose will be needed to displace the label the sensor has a higher detection limit, but in other words, the sensor's working range is increased. If the binding is weaker, even low concentrations of glucose will displace all the bound labels, the detection limit decreases. These are considerations that enter all competitive assays.

The main non-labelled optical technique that has come to recent commercial exploitation is evanescent field sensing in various forms surface plasma resonance (BIAcore and BIAlite from Pharmacia Biosensor[65]), resonating mirrors (IAsys from Fisons Applied Sensor Technology [66]) and grating couplers (BIOS-1 from Artificial Sensing Instruments [67]). When light is channelled along a surface or reflected multiply within a thin layer, the associated electromagnetic field penetrates some distance away from that surface, i.e. into the contacting medium, before decay-

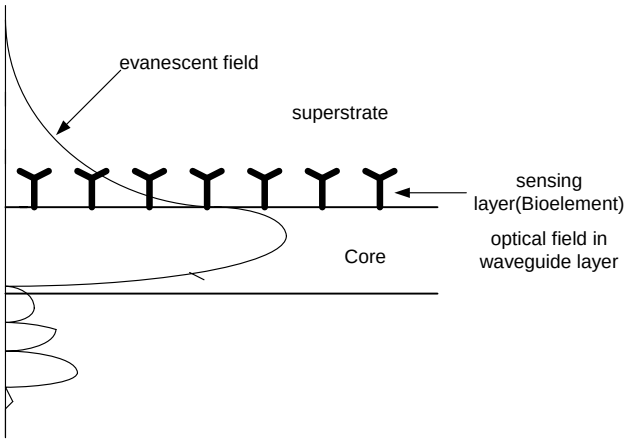

Figure 6.5: Non-Labelled optical sensor

ing completely 6.5. This means that matter at the medium/surface interface can interact with the evanescent field. Sensors based on this effect are sensitive to a parameter that combines mass and refractive index. Usually, one assumes that the refractive index of the medium at the sensor surface is more or less constant, and that changes in the signal are due to mass changes the devices essentially become mass sensors. The transition from sensor to biosensor comes about by immobilising a recognition layer of biological origin (for example, a layer of antibodies directed against the analyte of interest) at the optical surface, i.e. within the evanescent field. The binding of analyte changes the mass within the sensitive region and give a change in signal.

The strength and weakness of the system is its generality. Advantageously, just by changing one biological recognition layer for another, the same basic instrument can be used to detect a wide range of analytes. However, on the down side, be-

cause the system is a mass sensor, and the recognition layer is often already quite "heavy", the analyte has to be sufficiently large to induce a further, significant change. As a result, this type of system is best suited to detection of large analytes such as antibodies, viruses and bacteria, although smaller molecules can be detected by resorting to labelling techniques. Furthermore, if the sample to be analysed is very heterogeneous (like most samples of medical interest), non-specific adsorption of proteins to the optical surface is a real problem, necessitating sample filtration and dilution. Much work is being devoted to the development of sensing surfaces that decrease non-specific binding this work has much in common with the study of biocompatibility in order to favour specific over non-specific binding. Due to their sensitivity, their real-time response and overall versatility, biosensors based on evanescent waves have found favour with most of the world's leading pharmaceutical as research tools in a wide number of applications. In practical terms, their size (that of a small television set) makes them ideal laboratory items but despite progress in miniaturisation of lasers, the high cost (dozens of thousands of dollars) excludes any mass market use for the foreseeable future.

In summary, due to progress in fabrication techniques for fibre-optics and integrated optics, optical biosensors have become commercial products with wide applicability in the pharmaceutical and diagnostics research. Partly due to lessons learned from enzyme-based immunoassay techniques, optical biosensors can also perform immunoassays tests that have not yet been satisfactorily achieved by elec-

trochemical biosensors. However, penetration of mass markets such as point-of-care testing, home-testing and continuous monitoring remains some way off due to the still-prohibitive costs and complexity of such devices.

6.3.5 Array Biosensor

The Array Biosensors was developed for simultaneous analysis of multiple samples for multiple analytes. A patterend array of capture antibodies is immobilized on the surface of a planar waveguide (ARROW waveguide) and a sandwich immunoassay conducted using a cocktail of fluorescent tracer antibodies, upon excitation of the fluorescent label by evanescent field, a CCD camera detects the pattern of fluorescent antigen-antibody complexes on the sensor surface. Image analysis software correlates the position of fluorescent signals with the identity of the analyte.

6.3.6 Immunosensors

The bioelement of a sensor (which create recognition event) is almost always an enzyme or an antibody. When the later is the case, the device can be called an immunosensor [60] because the antibodies (also known as immunoglobulins) are an essential part of the body's immune system, and the device (waveguide) mimics that sytem by recognizing a specific antigen and generating a response to it, thus permitting measurement of the amount of anigen present.

6.3.7 Biochip

The biochip (A miniature, hand held biosensor which uses evanescent wave and planar technology with combination of other technologies) is a self-contained device which allows simultaneous detection of various types of Biotargets using different biorecepters (antibodies, nucleic acids, enzymes etc) on a single system (chip).

Biochip technologies could offer a unique combination of performance capabilities and analytical features of merit not available in any other bioanalytical system currently available. Biosensors and Biochips can be classified either by their bioreceptors or their transducer type see figure 6.6. These integrated biosensor arrays that use the same excitation source for all of the elements and the same measurement process have been termed many things: gene chips, DNA-chips, etc. Most of the different array chips have been based on the use of nucleic acids (i.e. DNA) as the bioreceptors. Other types of bioreceptors such as anti-bodies, enzymes and cellular components can also be used. It is noteworthy that substrates having microarrays of bioreceptors are often referred to as biochips although most of these systems do not have integrated microsensor detection systems. A few of he recent applications and advances will be briefly discussed.

An optical microarray system using a charge-coupled device (CCD) detector and DNA probes has been developed by Vo-Dinh and coworkers [61]. The evaluation of various system components developed for the DNA multi-array biosensor were

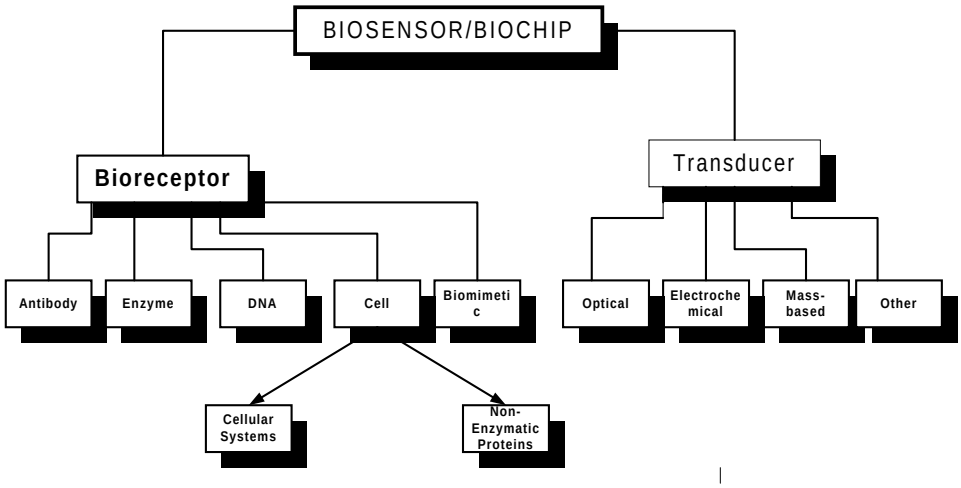

Figure 6.6: schematic of biosensor/biochip classification schemes

discussed. DNA probes labeled with visible and near infrared (NIR) dyes are evaluated. Examples of applications of gene probes in DNA hybridization experiments and in biomedical diagnosis (detection of the $p53$ cancer suppressor gene) illustrated the usefulness and potential of the DNA multiarray device. An optical microarray for the detection of toxic agents using a planar array of antibody probes was described by Ligler and coworkers [61]. Their system was composed of a CCD for detection, an excitation source and a microscope slide with a photoactivated optical adhesive. See figure 6.7 Antibodies against three different toxins, staphylococcal enterotoxin B (SEB), ricin and Yersinia pestis, were covalently attached to small wells in the slide formed by the optical adhesive. The microscope slide was then mounted over the CCD with a gradient refractive index (GRIN) lens array used to focus the wells onto the CCD. Toxins were then introduced to the slide followed by

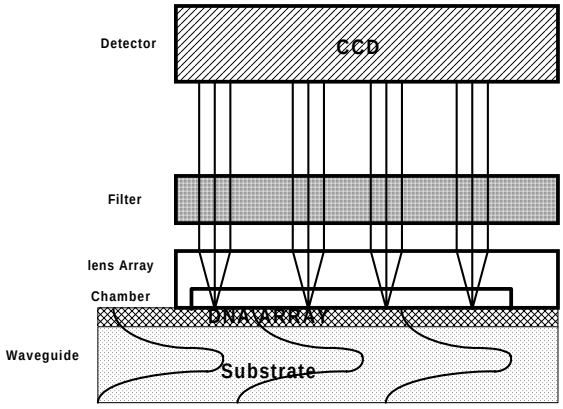

Figure 6.7: schematic of DNA Array detection

Cy5-labeled antibodies. The bound antibodies were then excited and the resulting fluorescence from all of the sensor locations were monitored simultaneously 6.7 This technology is so sophisticated that todays integrated Biochip is produced using the capability of fabricating multiple optical sensing elements and microelectronics for up to 100 sensing elements on a single chip [68]. Some integrating state of the art technologies such as Biochip, cell based assays and Bioinformatics, in combination with traditional Chinese medicine (TCM), are used for disease gene identification and drug discovery . The combination of these technologies will greatly accelerates the identification of disease related genes. This technology is so sophisticated that it provided the rapid, simple cost effective, selective and sensitive detection of biochemical substances (proteins, metabolics, nucleic acids), biological species or living system (bacteria, virus or related components) at ultra trace levels in biological

samples (tissues, blood , and other body fluids), which is very essential for handy diagnosis. Researches tested performance of biochip using fluorescence detection of both DNA probes specific to gene fragments of the mycobacterium Tuberculosis (TB) and the Human immuno deficiency virus (HIV) system and improved performance detected compared to previous techniques. For medical applications, this cost advantage will allow the development of extremely low cost, disposable biochips that can be used for in-home medical diagnostics of diseases without the need of sending samples to a laboratory for analysis. This technology is so fast developing that each and every research cannot be mentioned,it is reported that nearly 1500 papers have been published in biosensors and biochip from january 1998 to august 1999, [61].

Chapter 7

Method of lines Analysis of Gaussian Beam Coupling to Multi-Layer ARROW

7.1 Introduction

Optical power coupling is an important design problem in Optical fiber communication [69] and Integrated Optics [24]. There has been a considerable interest during the last two decades in the development of new means of increasing the efficiency of this process. A substantial portion of power can be lost in the region between the light source and the waveguide, making the analysis of the factors that influence the coupling efficiency of great importance. In conjunction with the rapid development

of integrated optics and optical waveguides in general, several numerical methods have been developed for the analysis of longitudinally-dependent effects in these waveguide structures. Among these methods are the Beam propagation Method (BPM) [14, 15], the Finite Difference Method [16] and the Method of lines (MOL) [11, 12].

In this work we will use the MOL for the analysis of the problem under consideration because of its simplicity, high accuracy, and its ability to account for back-scattered waves. In contrast to other numerical methods mentioned, this technique is very efficient with respect to computational time due to its semianalytical nature.

As will be explained in a subsequent section, light beams can be coupled to multi-layer ARROW planar waveguide structures using different techniques. These techniques include prism coupling [70], grating coupling [71], and endfire or butt coupling [72]. Of these different methods, end-fire or butt-coupling techniques, are of particular interest because of their several advantages such as ease of handling of in-line input and output beams [21]. It is therefore the purpose of this thesis to consider the analysis of endfire coupling of a normally incident Gaussian beam into a multi-layer ARROW using the MOL.

7.2 Coupling Techniques

As stated in the introductory section, light can be coupled from the laser source into a waveguide by either evanescent [73] or endfire coupling techniques [74]. Evanescent coupling methods include prism and grating coupling and utilize the interaction between the evanescent filed of the incident beam with the desired guided mode of the waveguide. Endfire or edge coupling involves shining the light beam directly or through a lens at the facet of the waveguide. Examples of the edge coupling are the endfire and butt coupling. In the following section we will only discuss endfire coupling. Other coupling techniques are well documented in [71, 21, 73]

7.2.1 Endfire/Butt coupling

Edge coupling which is excitation of a thin film waveguide directly from a laser source was first proposed by Marcuse and Marcatili [75] in 1971. Since then it has been investigated by several researchers [21, 76, 72, 73].

Examples of this coupling are endfire and butt coupling. In endfire coupling [77], light is focussed using a lens into the facet of a waveguide (see figure 7.1). Whereas in butt coupling light coupling, is achieved by attaching the source directly to the waveguide. This is illustrated in figure 7.2. In both techniques it is required that the incident field pattern matches that of the waveguide mode to be excited.

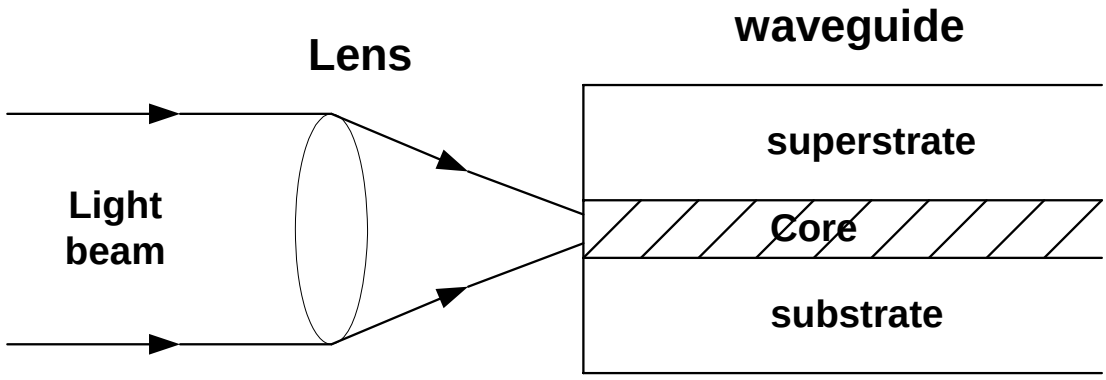

Figure 7.1: End-fire coupling

There are two main types of losses associated with edge coupling. One is power loss due to the miss-match between the incident field pattern and that of the guided modes. This is called radiation loss. The other is associated with the reflections from the coupled waveguide or Fresnel loss. The later can be reduced very dramatically by using antireflection coatings or an index-matching fluid. Other losses might arise if the film face is not perfectly flat.

Butt coupling has the advantage of design simplicity and structural compactness. The spacing between the light source and the waveguide must be reduced to the smallest possible value. Lateral, axial, and angular alignment must also be observed.

7.2.2 Statement of the Problem

Consider a gaussian beam having a spot size of w_0, incident normally on a multilayer ARROW planar waveguide positioned at $z = 0$. The lateral position of the beam axis

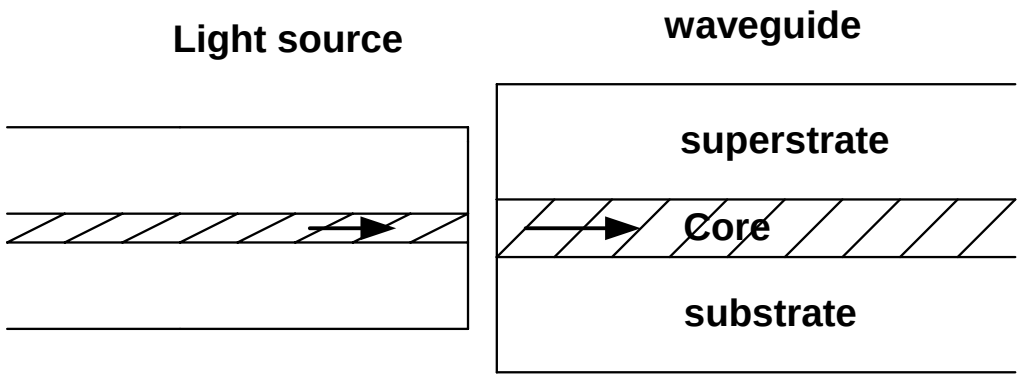

Figure 7.2: Butt-coupling

is located at distance x_0 from the waveguide axis. The MOL requires knowledge of the gaussian beam distribution at $z = 0$ only. This is given by the simple expression:

$$\psi = E_o \exp\left[-\frac{(x - x_o)^2}{w_o^2}\right] \tag{7.1}$$

Where E_0 is the beam amplitude at $x = x_0$. It is required to calculate the percentage of the beam power that will be coupled into the multi-layer planar waveguide, and the percentage of this power that will be guided and radiated. The launching conditions such as the values of w_0, and $x = x_0$ will be varied to realize the optimum conditions that will result in the highest coupling effciency.

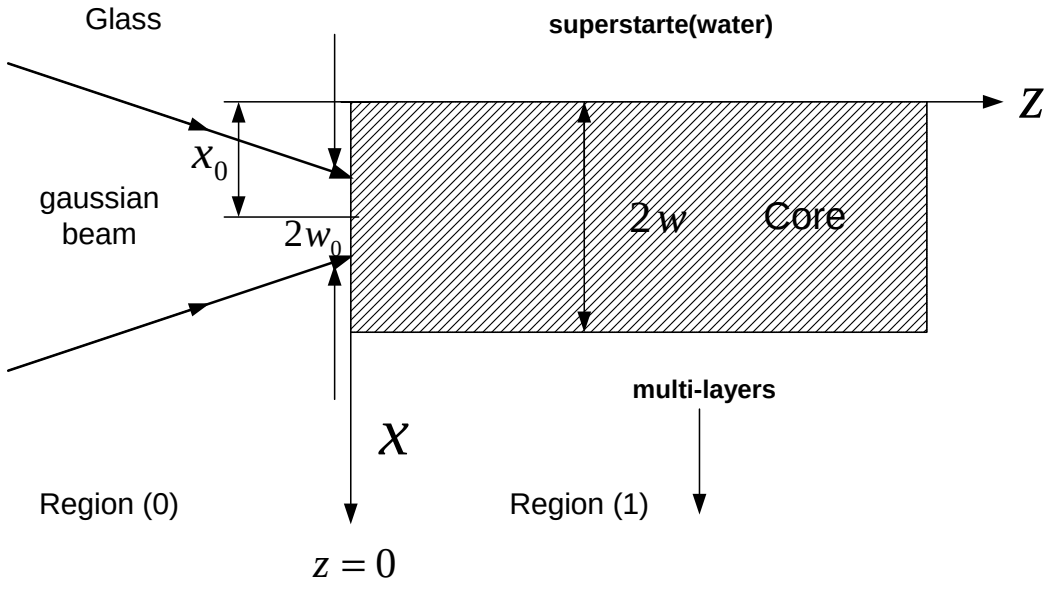

Figure 7.3: Coupling of Guassian beam into a Multi-layer ARROW

7.2.3 Calculation of Power Coupling Efficiency in Edge Coupling

Any general two-dimensional field $\psi(x, z)$ can be represented as a linear combination of a complete set of orthonormal modes, that is [21]:

$$\begin{aligned}\psi(x,z) &= \alpha_0 f_0(x)e^{j\beta_0 z} + \alpha_1 f_1(x)e^{j\beta_1 z} + \alpha_2 f_2(x)e^{j\beta_2 z} + \cdots + \alpha_m f_m(x)e^{j\beta_m z} + \cdots \\ &\quad + \alpha_M f_M(x)e^{j\beta_M z} + \int_v \alpha_v f_v(x)e^{j\beta_v z}dv \qquad (7.2)\end{aligned}$$

where α_m = mth-mode expansion coefficient, β_m = mth-mode propagation constant and $\int_v \alpha_v f_v(x)e^{j\beta_v z}dv$ represents an integration over the continuum of all radiation modes. The integer M represents the highest possible order of the guided modes.

The modal transverse profiles $\{f_m(x)\}$ describe a set of orthonormal functions over the transverse coordinate. For a single-mode waveguide ($M = 0$):

$$\psi(x,z) \;=\; \alpha_0 f_0(x) e^{j\beta_0 z} + \int_v \alpha_v f_v(x) e^{j\beta_v z} dv \tag{7.3}$$

At the input end of the waveguide ($z = 0$) the field ψ becomes:

$$\psi(x,0) \;=\; \alpha_0 f_0(x) + \int_v \alpha_v f_v(x) dv \tag{7.4}$$

By using the orthogonality relation between the modal fields, which is expressed as [78]:

$$\int_{-\infty}^{+\infty} \frac{f_m(x)}{K} f_n(x) dx = \begin{cases} 0 & for\ m \neq n \\ \int_{-\infty}^{+\infty} \frac{f_m^2(x)}{K} dx & for\ m = n \end{cases} \tag{7.5}$$

where K is defined as:

$$K = \begin{cases} n^2(x) & for\ TM\ modes \\ 1 & for\ TE\ modes \end{cases} \tag{7.6}$$

and $n(x)$ represents the refractive index distribution.

The modal coefficient α_m is given by [21]:

$$\alpha_m = \frac{\int_{-\infty}^{+\infty} \psi(x,0)\frac{f_m(x)}{K}dx}{\int_{-\infty}^{+\infty} \frac{f_m^*(x)f_m(x)}{K}dx} \tag{7.7}$$

Hence the coefficient of the fundamental mode α_0 is given by:

$$\alpha_0 = \frac{\int_{-\infty}^{+\infty} \psi(x,0)\frac{f_0(x)}{K}dx}{\int_{-\infty}^{+\infty} \frac{f_0^2(x)}{K}dx} \tag{7.8}$$

The power flowing in the z direction per unit length of the y direction is given by [79]:

$$P_z = \frac{1}{2}\int_{-\infty}^{+\infty} \mathrm{Re}(\mathbf{E}\times\mathbf{H}^*)_z dx = -\frac{1}{2}\int_{-\infty}^{+\infty} E_y H_x^* dx \tag{7.9}$$

Our main objective here is to calculate the efficiency of power coupling from a laser source into a multi-layer ARROW. Coupling efficiency is defined as the ratio of the

guided power to the incident power, or

$$\eta = \frac{P_g}{Pi} \tag{7.10}$$

For detailed derivation of the calculation of the coupling efficiency see reference [21]. Here we will only state the final form and apply the results. The coupling efficiency for the mth guided mode in endfire coupling can be described by the following overlap integral

$$\eta = \frac{\left|\int_{-\infty}^{\infty} \psi_t(x) \cdot f_m^*(x)dx\right|^2}{\int_{-\infty}^{\infty} f_m(x) \cdot f_m^*(x)dx \int_{-\infty}^{\infty} \psi_i(x) \cdot \psi_i^*(x)dx} \tag{7.11}$$

It has been assumed in equation 7.11 that the end surface of the waveguide has an effective anti-reflection coating and the reflection losses are negligible. For the purpose of our treated waveguide, we cannot neglect the reflected power since the difference between the refractive indices of the waveguide and media incidence is considerable.

7.2.4 The application of the MOL to the Coupling Problem

The MOL main principles introduced and the mathematical relations developed in the previous chapters (refer chapter and section number) will be applied in this sec-

tion to analyze the coupling of an incident field into the multi-layer ARROW.

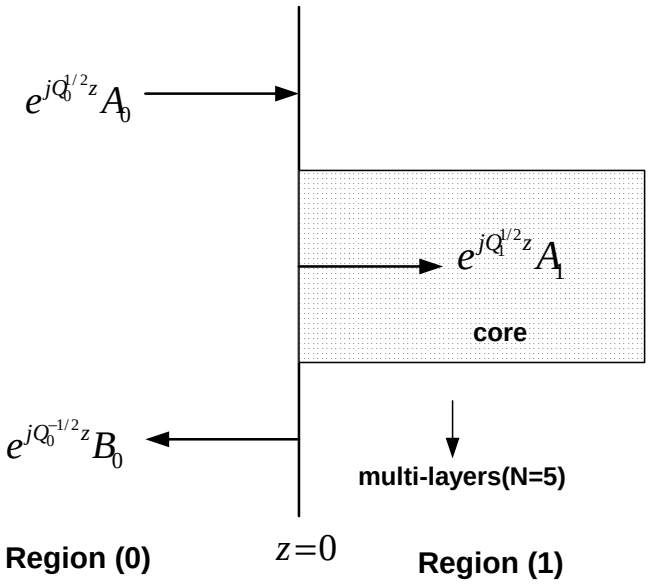

Figure 7.4: The incident, reflected and transmitted fields using the MOL

Figure 7.4 depicts a field incident from glass; region (0), into a multi-layer ARROW; region (1). The field in region (0) is described by two terms: $e^{jQ_o^{1/2}z}A_o$ which represents that part of the field propagating in the postive z-direction, and $e^{-jQ_o^{1/2}z}B_o$ which represents the reflected field propagating in the negative z-direction. In region (1) there is only a transmitted field described by the term $e^{jQ_o^{1/2}z}A_1$.

A fraction of the incident field power will be transmitted to region (1) and the rest will be reflected backwards to region (0). Part of the transmitted power will be coupled to the guided modes of the multi-layer ARROW waveguide. The other part of the transmitted power will be coupled to radiation modes and thus will be radiated. Based on the above and following equation (mention), the fields in region (0); Ψ_0

and in region (1); Ψ_1 can be expressed as:

$$\Psi_0 = e^{+jQ_0 z} A_0 + e^{-jQ_0 z} B_0 \tag{7.12}$$

$$\Psi_1 = e^{+jQ_1 z} A_1 \tag{7.13}$$

where Ψ is a column vector containing the sampled fields. A_0, B_0 and A_1 are constant vectors. For TE polarization, Ψ is continuous at the interface at $z = 0$, that is $\Psi_0|_{z=0} = \Psi_1|_{z=0}$. From equations 7.12 and 7.13, we have:

$$A_0 + B_0 = A_1 \tag{7.14}$$

continuity of $\frac{d}{dz}\Psi_0$ at $z = 0$, yields:

$$\frac{d}{dz}\Psi_o = \frac{d}{dz}\Psi_1 \tag{7.15}$$

equation 7.15 is valid only for TE waves.

Differentiating equations 7.12 and 7.13 with respect to z leads to:

$$\Psi_0^{'} = jQ_0^{1/2} e^{jQ_0^{1/2}z} A_0 - jQ_0^{1/2} e^{-jQ_0^{1/2}z} B_0 \tag{7.16}$$

and

$$\Psi_1^{'} = jQ_1^{1/2} e^{jQ_1^{1/2}z} A_1 \tag{7.17}$$

results in:

$$jQ_0^{1/2} e^{jQ_0^{1/2}z} A_0 - jQ_0^{1/2} e^{-jQ_0^{1/2}z} B_0 = jQ_1^{1/2} e^{jQ_1^{1/2}z} A_1 \tag{7.18}$$

substituting $z = 0$; in the previous equation, we have

$$Q_0^{1/2} A_0 - jQ_0^{1/2} B_0 = Q_1^{1/2} A_1 \tag{7.19}$$

B_0 can be eliminated by adding equations 7.14 and 7.19, we have:

$$2A_0 \;\; = \;\; (I + Q_0^{-1/2} Q_1^{1/2}) A_1 \tag{7.20}$$

$$A_1 = 2(I + Q_0^{-1/2} Q_1^{1/2})^{-1} A_0 \tag{7.21}$$

and

$$B_0 = (I - Q_0^{-1/2} Q_1^{1/2})(I + Q_0^{-1/2} Q_1^{1/2})^{-1} A_0 \tag{7.22}$$

Where I is the identity matrix. The incident field at $z = 0$; A_0 is known from 7.20 and the reflected field can be obtained using equation 7.22. Therefore, the transmitted field at $z = 0$; A_1 can be calculated from equation 7.21.

7.2.5 Calculation of Power coupling efficiency using the MOL

Consider the illustration of the coupling problem depicted in figure 7.4. The electric field continuity at $z = 0$ implies that

$$\psi_i + \psi_r = \psi_t \tag{7.23}$$

where ψ_t is the transmitted field (region (1)),and ψ_i and ψ_r are the incident and reflected field (region (0)) respectively. Our aim here is to find the percentage

of power coupled to the fundamental mode of the waveguide. Endfire coupling efficiency to the fundamental mode depends mostly on the spatial overlap between the incident beam and the mode. As in section 7.2.3, the power coupling efficiency is defined as:

$$\eta = \frac{P_g}{P_i} = \frac{\mathrm{Re}\int_{-\infty}^{\infty} E_{y_g} \cdot H_{x_g}^* dx}{\mathrm{Re}\int_{-\infty}^{\infty} E_{y_i} \cdot H_{x_i}^* dx} \tag{7.24}$$

In the MOL, the incident electric field is given by

$$E_{y_i} = e^{jQ_0^{1/2}z} A_0 \tag{7.25}$$

where the $M \times 1$ column matrix, A_0, represents the incident field at $z = 0$ and the $M \times M$ matrix where Q_0 is defined in chapter 3. Using Maxwell's equations, the incident magnetic field is given by:

$$H_{x_i} = \frac{j}{\omega\mu}\frac{\partial}{\partial z}(e^{+jQ_0^{1/2}z} A_0) \tag{7.26}$$

$$= -\frac{Q_0^{1/2}}{\omega\mu} e^{+jQ_0^{1/2}z} A_0 \tag{7.27}$$

and

$$H_{x_i}|_{z=0} = -\frac{1}{\omega\mu} Q_0^{1/2} A_0 \tag{7.28}$$

The incident average power flow is given by:

$$P_i = \frac{1}{2} Re \int_{-\infty}^{\infty} E_{y_i} H_{x_i}^* dx \tag{7.29}$$

For discrete samples, integration is replaced by summation over the index of the array.

$$P_i = -\frac{1}{2} \mathrm{Re}\Big\{ \sum_{m=1}^{M} E_{y_i}(m) H_{x_i}^*(m) \cdot \overline{\Delta x}_m \Big\} \tag{7.30}$$

$$P_i\Big|_{z=0} = \frac{1}{2\omega\mu} \mathrm{Re}\Big\{ (Q_0^{1/2} A_o)^* A_o \cdot \overline{\Delta x}_m \Big\} \tag{7.31}$$

For uniform mesh, Δx_m is constant for all layers but for non-uniform mesh, Δx_m is different for each layer.

similarly, the transmitted field is given by

$$E_{y_t} = e^{j Q_1^{1/2} z} A_1 \tag{7.32}$$

Where the vector A_1 represents the transmitted field at $z = 0$. Following equation

7.8, the fundamental mode excitation coefficient expressed as:

$$\alpha_0 = \frac{A_1^t F_0}{F_0^t F_0} \tag{7.33}$$

where the $M \times 1$ vector F_0 represents the discretized modal field distribution in region (1), A_1^t and F_0^t are the transposed forms of the matrices A_1 and F_0 respectively. The guided electric field of the fundamental mode is therefore equal to

$$E_{y_g} = \alpha_0 F_0 \tag{7.34}$$

from which the corresponding magnetic field can be written as

$$H_{x_g} = \frac{-1}{2\omega\mu}(Q_1^{1/2} \cdot \alpha_0 F_o) \tag{7.35}$$

The average guided power is given by:

$$P_g\Big|_{z=0} = \frac{1}{2\omega\mu}\mathrm{Re}\Big\{(Q_1^{1/2} \cdot \alpha_o F_o)^* \cdot \alpha_o F_o \cdot \overline{\Delta x}_m\Big\} \tag{7.36}$$

As a result, the power coupling efficiency for TE polarized waves at $z = 0$, can be written in the following discretized form:

$$\eta = \frac{\mathrm{Re}\Big\{(Q_1^{1/2} \cdot \alpha_o F_o)^* \cdot \alpha_o F_o \cdot \overline{\Delta x_m}\Big\}}{\mathrm{Re}\Big\{(Q_0^{1/2} A_o)^* A_o \cdot \overline{\Delta x_m}\Big\}} \tag{7.37}$$

7.2.6 Convergence of the MOL

The validity of the MOL result can be checked by monitoring power conservation at the coupling boundary. The ratio of the reflected power to the incident power, R is defined as:

$$R = \frac{P_r}{P_i} \tag{7.38}$$

Similarly, the ratio of the transmitted power to the incident power, T is defined as:

$$T = \frac{P_t}{P_i} \tag{7.39}$$

In order to have conservation of power , R and T must sum to unity i.e.,

$$R + T = 1 \tag{7.40}$$

7.2.7 Results

In order to have maximum coupling efficiency using a gaussian beam as input one needs to take care of many parameters. One of which is power conservation at the coupling boundary which is discussed in the previous section. Coupling a gaussian beam to a leaky waveguide is not an easy task, specially to multi-layer ARROW waveguide. Before coupling we have to make sure that the multi-layer ARROW is synchronized with respect to PML tunning, power loss (db/cm), superstrate thickness, Mesh size and number of discretization lines for a particular core width. And it should be noted that all these parameters will change as we change the core width. The next step after this is to align the gaussian beam for maximum coupling and for this we have chosen a wide core width ($0.81\mu m$) and by trial and error procedure we started by keeping $x_0 = 0$ and varied the spot size (w_0) and checked for power balance at the boundry that is $R + T = \frac{\mathrm{P}_t + \mathrm{P}_r}{\mathrm{P}_i} = 1$, and we have noted that to get good power balance we have to vary both the parameters simultaneously and we have maintained a good power balance, that is the difference term ϵ (where $\epsilon = \frac{\mathrm{P}_t + \mathrm{P}_r}{\mathrm{P}_i} - 1$) has values between 2.3×10^{-04} and 8.5×10^{-05}. This process is very tedious and one never knows when and what parameters will provide good power balance, as we match the input beam to the fundamental mode of the waveguide. Not only power balance should be monitored but we have to make sure that the peak of the beam should be inside the core to make sure that MOL is stable for

particular spot size and lateral position.

Label	Spot size $w_0(\mu m)$	Lateral Position $x_0(\mu m)$	Coupling Efficiency (%)
A	0.19	0.22	70
B	0.2	0.22	73.4
C	0.21	0.22	74.7
D	0.22	0.22	75.87
E	0.23	0.22	76.84
F	0.24	0.22	77.68
G	0.25	0.22	76

Table 7.1: Coupling Efficiency Versus Spot Size for $t_c = 0.40\mu m$

Label	Spot size $w_0(\mu m)$	Lateral Position $x_0(\mu m)$	Coupling Efficiency (%)
A	0.24	0.1	72.3
B	0.24	0.15	74.45
C	0.24	0.18	75.74
D	0.24	0.2	76.63
E	0.24	0.21	77.21
F	0.24	0.22	77.68
G	0.24	0.24	77.17

Table 7.2: Coupling Efficiency Versus Lateral postion for $t_c = 0.40\mu m$

In order to provide insight of coupling problem, we have plotted the maximum coupling efficiency versus spot size for a core size $t_c = 0.4\mu m$, and one can infer from figure 7.5 that for a particular spot size ($0.24\mu m$) one gets the maximum coupling efficiency. Points A,B,C,D,E and F in figure 7.5 shows the maximum coupling efficiency for a paricular spot size and they are tabulated in table 7.1. Figure 7.6

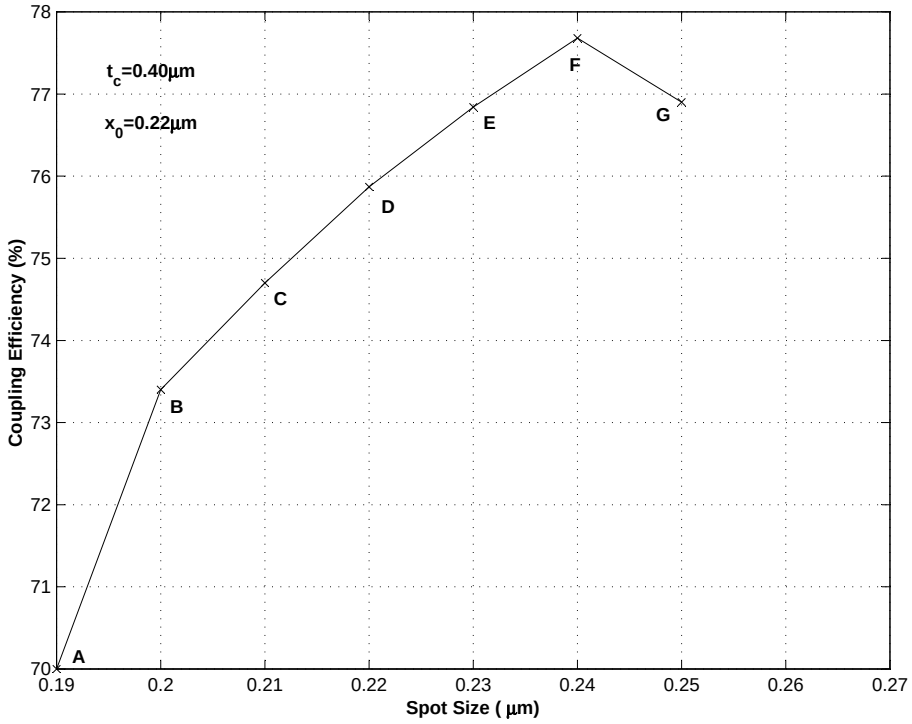

Figure 7.5: Coupling Efficiency Versus Spot Size (w_0)

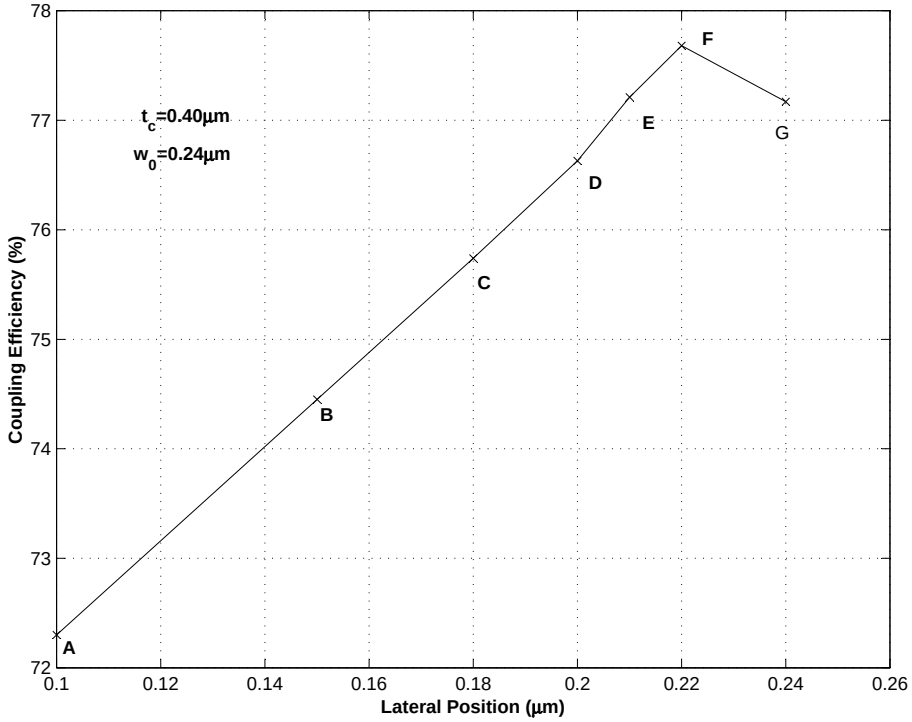

Figure 7.6: Coupling Efficiency Versus Lateral Position (x_0)

Label	Core Thickness (μm)	Lateral Position $x_0(\mu m)$	Spot size $w_0(\mu m)$	Coupling Efficiency (%)
A	0.21	0.06	0.095	42.31
B	0.3	0.11	0.13	60
C	0.4	0.22	0.24	77.68
D	0.5	0.23	0.19	85
E	0.81	0.3	0.34	98.64

Table 7.3: Maximum Coupling Efficiency Versus Core Thickness with Optimum Lateral Position and Optimum Spot Size

show the variation of the coupling efficiency versus lateral position, it is clear that at $x_0 = 0.22\mu m$ we get maximum coupling efficiency and the points A,B,C,D,E and F are tabulated in table 7.2. So, for a core size of $0.40\mu m$, $w_0 = 0.24\mu m$ and $x_0 = 0.22\mu m$, we get the maximum coupling efficiency. This procedure is repeated for all core widths shown in table 7.3.

We got a coupling efficiency of 98.64% for a wide core ($t_c = 0.81$) and 42.31% for narrow core width ($t_c = 0.21$). The plot for maximum coupling efficiency versus core width is shown in figure 7.7. From the figure one can infer that as the core size increases from $t_c = 0.21$ to $t_c = 0.81$ the maximum coupling efficiency is approximately doubled. The points A,B,C,D,E on the figure shows the efficiency for a particular core width and they are tabulated in table 7.3. One interested observation that can be noted from the table is the values of x_0, which gave maximum efficiency. The values of x_o is very close to the center of the core, and which is not obvious if one sees the highly unsymmetric nature of the waveguide.

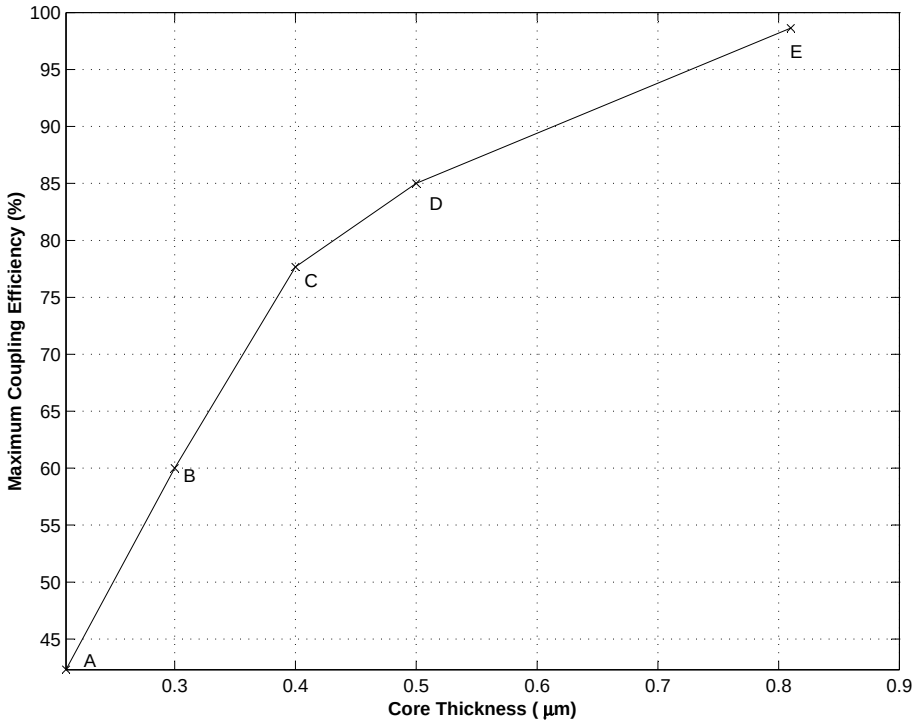

Figure 7.7: Maximum Coupling Efficiency Versus Core Thickness (t_c)

Chapter 8

Summary, Conclusions and Future Work

In this thesis, the Method of lines with higher-order approximation has been applied to find modal profile and propagation constants of the eigen-modes of different multi-layer optical waveguide structures (high contrast symmetric waveguide, basic ARROW waveguide, multi-layer ARROW).The MOL is applied successfully to analyze a multi-layer ARROW waveguide used for evanescent filed enhancement. This includes power loss for TE and TM modes, sensitivity analysis and coupling efficiency using endfire excitation. A brief description of the work done, followed by conclusion and some future extensions of this work is given below.

8.1 Summary

- The MOL with higher-order approximations, five-point and seven-point approximations, is implemented for different structures and the results are verified against both published and analytical results.

- Perfectly Matched Layer (PML) absorbing boundary scheme has been used extensively in thisthesis. In chapter 4, 5, 7, a double layer PML is applied to absorb the radiative field.

- The MOL is used to find the modal fields and effective indices of the TE, TM ARROW waveguide modes. The use of appropriately tuned PML gives correct open-space approximation for leaky modes of the ARROW, thus giving accurate estimation of the effective indices (real and imaginary part) of different modes. These MOL results are verified against published as well as analytical results.

- The multi-layer ARROW waveguide is used with N=5 layer which gave us TE_0 power loss below $0.1db/cm$ for small core thickness. The evanescent field enhancement in low-index superstrate increases as we decreases the core thickness, which also increases the sensitivity but decreases the maximum coupling efficiency. Hence there must be a compromise between evanescent field enhancement in the low-index superstrate and coupling efficiency. This com-

promise depends on the particular application used and will not be addressed here.

8.2 Conclusions

- The three-point, five-point and seven-point approximations are used in the MOL to model a waveguide structure and it is found that the higher-order approximation requires relatively few discretization lines to sample the problem space. As shown in chapter 3, the higher-order approximation gives more accurate estimation of the modal field and the effective index.

- The excellent performance of PML in simulating infinite space at the mesh boundry is evident from the ARROW waveguide modeling exercise in chapter 4 and chapter 5. The power loss factor (imaginary part of the effective index)is accurately predicted by MOL for different ARROW modes. This shows the excellent absorption of the leaky waves by the PML in the substrate region of ARROW. As shown in chapter 4, the performance of the PML can be improved by decreasing the mesh size in the first PML layer and using coarser mesh in the second PML layer to simulate a relatively thicker absorber.

- The PML is applied in conjunction with MOL to analyze the multi-layer ARROW, the excellent performance of PML is evident from the study of polarization properties and sensitivity analysis. It is evident that the sensitivity and

power enhancement of the evanescent field in the low-index superstrate of the multilayer ARROW waveguide is sufficiently increased as the core thickness is decreased.

- The gaussian beam coupling problem which involves a single discontinuity, has been solved using the MOl. The maximum coupling efficiency is increases with the core thickness of the multi-layer ARROW waveguide.

8.3 Future Prospects

The following is a brief list of suggestions for possible future work in this area.

- Spectral response of the multi-layer ARROW can be studied using water or any other substance as low-index superstrate.

- In this thesis we have analyzed the multi-layer ARROW waveguide for N=5 pairs since this choice results in reducing the loss of the TE_0 mode to below $0.1dB/cm$ for small core thicknesses. We also have shown that the structure behaves as TE pass polarizer. This structure can be studied by increasing the number of pairs and we expect that, as N increases the waveguide will pass both TE and TM polarizations.

- Periodic corrugation can be introduced on the top surface of multi-layer ARROW resulting in multi-layer ARROW grating. And this structure can be used

as wavelength selective filter due to multiple reflections from each discontinuity and their interaction with each other to cause resonance or anti-resonance in the propagation direction. We can also analyze this structure for modal spectral response for different groove depths, different number of periods and different loss of the ARROW.

- As it has been showed that the multi-layer ARROW waveguide provides large enhancement of the evanescent field. If a movable lossy element, let us say made of Si ($n_e = 3.85 + j0.019$). Moving the element closer to the core layer will result in leakage of light from the waveguide to the element which will then be absorbed. This device can offer a bulk attenuation of the order of 5 digits. When the element is moved away the attenuation can be made very small as the evanescent field does not encounter the the element. Therefor, this device can be used as a mechno-optical waveguide on/off switch, where the absorbing element is moved into and out of the evanescent field of the guided mode in order to achieve switching. This device can be used for channel selection purposes in integrated optical sensor arrays.

- In this thesis we have analyzed the power coupling efficiency for different core sizes to the multi-layer planar ARROW waveguide. In future, output coupling loss can be analyzed using the MOL.

- In this thesis gaussian beam coupling to multi-layer ARROW is obtained by

using water as the low-index superstrate and glass is used in region 0 of figure 7.3. The same structure can be analyzed with air the as low-index superstrate as well in region 0.

Bibliography

[1] S. E. Miller, "Light propagation in generalized lenslike media," *Bell Syst. Tech. Journal*, vol. 44, pp. 2017–2064, 1965.

[2] S. E. Miller, "Integrated optics: an introduction," *Bell Syst. Tech. Journal*, vol. 48, pp. 2059–2069, 1969.

[3] A. N. Weiping Huang, Raed M. Shubair and Y. L. Chow, "The modal characteristics of ARROW structures," *Journal of Lightwave Technology*, vol. 10, pp. 1015–1022, August 1992.

[4] J. Kubica, "Modal propagation within ARROW waveguides," *Optics Communications*, vol. 78, pp. 133–136, August 1990.

[5] T. L. K. M. A. Duguay, Y. Kokubun and L. Pfeiffer, "Antiresonant reflecting optical waveguides in $SiO_2 - Si$ multilayer structures," *Applied Physics Letters*, vol. 49, pp. 13–15, July 1986.

[6] T. Baba, Y. Kokuban, T. Sakaki, and K. Iga, "Loss reduction of an ARROW waveguide in shorter wavelength and its stack configuration," *Journal of Lightwave Technology*, vol. 6, pp. 1440–1445, September 1988.

[7] J. M. Kubica, A. Malag, J. Gazecki, M. W. Austin, and G. K. Reeves, "AlGaAs/GaAs ARROW waveguides," *Electronics Letters*, vol. 29, pp. 1058–1060, June 1993.

[8] J. L. Archambault, R. J. Black, S. Lacroix, and J. Bures, "Loss calculations for antiresonant waveguides," *Journal of Lightwave Technology*, vol. 11, pp. 416–423, March 1993.

[9] H. Jamid, "A multi-layer arrow channel wave-guide for evanescent field enhancement in low index media," *sent for possible publication in the IEEE Journal of light wave technology*, March 2001v.

[10] A. K. Taneja and A. Sharma, "Reflection characteristics of guided wave bragg gratings using the collocation method," *SPIE Proceedings, Internationl conference on fiber optics and photonics*, vol. 3666, pp. 112–119, April 1999.

[11] J. Gerdes and R. Pregla, "Beam-propagation algorithm based on the method of lines," *Optical Society of America (B)*, vol. 8, pp. 389–394, Feb. 1991.

[12] U. Rogge and R. Pregla, "Method of lines for the analysis of strip-loaded optical waveguides," *Optical Society of America (B)*, vol. 8, pp. 459–463, Feb. 1991.

[13] Q.-H. Liu and W. C. Chew, "Analysis of discontinuities in planar dielectric waveguides : An eigenmode propagation method," *IEEE Transactions on Microwave Theory and Techniques*, vol. 39, pp. 422–430, Mar. 1991.

[14] C. L. Xu and W. P. .Huang, *Finite-Difference Beam-Propagation Methods for Guided Wave optics*. Progress in Electromagnetics Research (PIER) 11, Elsevier Science Publishing Co., Inc., 1995.

[15] H. M. Masoudi, M. Al-Sunaidi, and J. M. Arnold, "Time-domain finite-difference beam propagation method," *IEEE Photonics Technology Letters*, vol. 11, pp. 1274–1276, Oct. 1999.

[16] S. T. Chu and S. K. Chaudhrui, *Finite-Difference-Time-Domain Methods for Optical Waveguide Analysis*. Progress in Electromagnetics Research (PIER) 11, Elsevier Science Publishing Co., Inc., 1995.

[17] K. S. Chiang, "Review of numerical and approximate methods for the modal analysis of general optical dielectric waveguides," *Optical and Quantum Electronics*, vol. 26, pp. 113–134, 1994.

[18] H. J. W. M. Hoekstra, "On beam propagation methods for modelling in integrated optics," *Optical and Quantum Electronics*, vol. 29, pp. 157–171, 1997.

[19] A. Sharma, *Collocation Method For Wave Propagation Through Optical Waveguiding Structures*. Progress in Electromagnetic Research, (PIER) 11, Elsevier Science Publishing Co., Inc., 1995.

[20] M. A. A. Pudensi and L. G. Ferreira, "Method to calculate the reflection and transmission of guided modes," *Journal of Optical Society of America*, vol. 72, pp. 126–130, 1982.

[21] M. J. Al-Majid, "Method of lines analysis of gaussian beam coupling to the dielectric slab waveguide," Master's thesis, King Fahd University of Petroleum and Minerals, Saudi Arabia, February 1994.

[22] M. N. Akram, "Analysis of anti-resonant reflecting optical waveguide (ARROW) grating using the method of lines," Master's thesis, King Fahd University of Petroleum and Minerals, Saudi Arabia, April 2000.

[23] S. J. Al-Bader and H. A. Jamid, "Perfectly matched layer absorbing boundary conditions for the method of lines modeling scheme," *IEEE Microwave and Guided Waves Letters*, vol. 8, pp. 357–359, November 1998.

[24] M. J. Adams, *An Introduction to Optical Waveguides.* John Wiley and Sons Inc., 1981.

[25] A. Yariv, *Optical Electronics.* Saunders College Publishing, 4 ed., 1991.

[26] J. A. Kong, *Electromagnetic Wave Theory.* John Wiley and Sons Inc., 1986.

[27] T. Tamir, ed., *Guided-Wave Optoelectronics*, vol. 26. Springer Series, 2nd ed., 1990.

[28] D. Marcuse, *Theory of Dielectric Optical Waveguides.* Academic Press Inc., 1974.

[29] M. A. Khan, "Analysis of metal-clad tm-pass polarizers using the method of lines," *M.s Thesis King Fahd university of petrolem and Minerals*, Feb 2001.

[30] Y. P. Chiou and H. C. Chang, "Analysis of optical waveguide discontinuities using pade approximation," *IEEE Photonics Technology Letters*, vol. 9, pp. 964–966, 1997.

[31] J. Gerdes, B. Lunitz, D. Benish, and R. Pregla, "Analysis of slab waveguide discontinuities including radiation and absorption effects," *Electronics Letters*, vol. 28, p. 1013, May 1992.

[32] W. D. Yang and R. Pregla, "Method of lines for analysis of waveguide structures with multidiscontinuities," *Electronics Letters*, vol. 31, p. 892, May 1995.

[33] R. Pregla and W. Yang, "Method of lines for analysis of multilayered dielectric wavegides with bragg gratings," *Electronics Letters*, vol. 29, p. 1962, October 1993.

[34] R. Pregla and E. Ahlers, "Method of lines for analysis of discontinuities in optical waveguides," *Electronics Letters*, vol. 29, p. 1845, October 1993.

[35] A. A. Shittu, *Study of periodic waveguides by the finite-difference time-domain method and the Method of Lines.* PhD thesis, King Fahad University of Petroleum and Minerals, Dhahran 31261, Saudi Arabia, September 1994.

[36] T. Itoh, ed., *Numerical Techniques for Microwave and Millimeter-Wave Passive Structures.* John Wiley and Sons Inc., 1989.

[37] S. J. Al-Bader and H. A. Jamid, "Method of lines applied to non-linear guided waves," *Electronics Letters*, vol. 31, pp. 79–85, Feb. 1995.

[38] M. Imtaar and S. J. Al-Bader, "Analysis of diffraction from abruptly-terminated optical fibers by the method of lines," *Journal of Lightwave Technology*, vol. 13, pp. 137–141, Feb. 1995.

[39] E. Ahlers and R. Pregla, "3-D modeling of concatenations of straight and curved waveguides by MoL-BPM," *Optical and Quantum Electronics*, pp. 151–156, 1997.

[40] W. D. Yang and R. Pregla, "The method of lines for analysis of integrated optical waveguide structures with arbitrary curved interfaces," *Journal of Lightwave Technology*, vol. 14, pp. 879–884, May 1996.

[41] F. H. Al-Harbi, "Implementation of a full vectorial method of lines analysis in the study of metal clad rib waveguide," Master's thesis, King Fahd Univeristy of Petroleum and Minerals, Saudi Arabia, December 2000.

[42] H. A. Jamid and M. N. Akram, "A new higher-order finite-difference approximation scheme for the method of lines," *IEEE Journal of Lightwave Technology*, March 2001. accepted for publication.

[43] Miyagi and Nishida, "a proposal for low loss leaky waveguide for submillimeter waves transmission," *IEEE Trans.*, vol. 28, p. 398, 1980.

[44] M. et al., "Remotly switch hollow-core antiresonant reflecting optical waveguide," *Opt. Lett.*, vol. 16, p. 1738, 1991.

[45] J. C. Wenyan Jiang and M. Fontaine, "Analysis of ARROW waveguides," *Optics Communications*, vol. 72, pp. 180–186, July 1989.

[46] J. M. Kubica, J. Gazecki, and G. K. Reeves, "Multimode operation of ARROW waveguides," *Optics Communications*, vol. 102, pp. 217–220, October 1993.

[47] Z. M. Mao and W. P. Huang, "An ARROW optical wavelength filter: Design and analysis," *Journal of Lightwave Technology*, vol. 11, pp. 1183–1188, July 1993.

[48] E. S. Tony and S. K. Chaudhuri, "An ARROW directional coupler acousto-optic filter," *Antennas and Propagation Society International Symposium, AP-S Digest*, vol. 2, pp. 1362–1365, 1994.

[49] V. Delisle, U. Trutschel, H. Tremblay, M. A. Duguay, and F. Lederer, "High finesse wavelength selective coupler based on ARROW," *IEEE Photonics Technology Letters*, vol. 8, pp. 791–793, June 1996.

[50] H. A. Jamid, "Frequency-Domain PML layer based on the complex mapping of space boundary condition treatment," *IEEE Microwave and Guided Wave Letters*, vol. 10, pp. 356–358, Sep. 2000.

[51] K.Remley and A. Weisshaar, "Design and analysis of silicon- based antiresonant reflecting optical wave-guide chemical sensor," *Optics letters*, vol. 21, pp. 1241–1243, August 1996.

[52] K. S. S.Kang and H. Minamitani, "Sensitivity analysis of a thin film optical waveguide biochemical sensor using evanescent field," *Applied Optics*, vol. 32, pp. 3544–3549, July 1993.

[53] A. D. J.F Govin and B. MacCraith, "Florescence capture by planar waveguide as platform for optical sensors," *Electronics letter*, vol. 34, pp. 1685–1687, 1998.

[54] D. J. A. C. F. Prieto, A. Llobera and L. Lechuga, "Design and analysis of silicon antiresonant reflecting optical waveguides for evanescent field sensor," *Journal of Lightwave Tech*, vol. 18, pp. 966–972, July 2000.

[55] O. Parriaux and G. veldhuis, "Normalized analysis for the sensitivity optimization of integrated optical evanescent-wave sensors," *Journal of light wave Technology*, vol. 16, pp. 573–582, April 1998.

[56] J. P. U. H. J. I. B.J Luff, James S. Wilkinson and N. Fabricius, "Integrated optical mach-zehender biosensor," *Journal of light wave Technology*, vol. 16, pp. 583–592, April 1998.

[57] "chapter 6: Optical biosensors," *www.age.psu.edu/dept/fac.htm*, pp. 1–14.

[58] B. Culshaw and J. Dakin, "Optical fibre sensors: systems and applications," *Artech house,Inc*, vol. 2, 1997.

[59] A. W. Szumlas, "High resolution distributed fiber optic sensors," *Indiana univeristy laboratory for spectrochemistry, Chemical sensing*, p. 1 of 2, may 2001.

[60] *www.fraserclan.com/biosens7.htm*, no. 6.

[61] T. Vo-dinh and B. cullum, "Biosensors and biocips: Advances i biological and medical diagnostics," *Anal Chem*, pp. 540–551, 200.

[62] A. g. J E Pearson and P. Vadgama, "Analytical aspects of biosensors," *Ann Clin Biochem*, pp. 119–145, 2000.

[63] D. Fraser, "Glucose biosensors- the sweet smell of success," *Medical Device Technology*, Sept 1994.

[64] M. L. . O. W. W. Trettnak, "Fiber-optic glucose sensor with a ph-optrode as the transducer," *Biosensors*, pp. 15–26, april 1988.

[65] D. L. M. . J. S. Schultz, "Design, manufacture and characterization of an optical-fibre glucose affinity sensor-based on a homogeneous fluorescence energy-transfer assay system," *Anal. Chim. Acta*, pp. 21–30, January 1993.

[66] U. J. et al., "Real time biospecific interaction analysis using surface plasmon resonance and a sensor chip technology," *Biotechniques*, pp. 620–625, Nov 1991.

[67] C. R. L. H. J. Watts and D. V. Pollard-Knight, "Optical biosensor for monitoring microbial cells," *Anal. Chem.*, pp. 2465–2470, Nov 1994.

[68] K. levon et al., "Biochip, tecnology development and applications," *Polytechnic university, Brooklyn, NY, USA*, 2001.

[69] M.Saruwatari and K.Nawata *Appl. Optics*, no. 11, pp. 1847–1856.

[70] D. sarid *Appl. Optics*, no. 18, pp. 2921–2926.

[71] S. T. Peng and T. Tamir, "TM mode perturbation analysis of dielectric gratings," *Applied Physics*, vol. 7, no. 35, pp. 35–38, 1975.

[72] A. Yariv, "Periodic structures for integrated optics," *IEEE Journal of Quantum Electronics*, vol. 14, pp. 233–253, Apr. 1977.

[73] C. H.Ribot, Sansonetti, "Improved design for the monolithic integration of laser and optical waveguide coupled by an evanescent field," *J. Quantum Electron*, vol. 26, no. 11, pp. 1930–1941, 1990.

[74] G. H. W.K Burns, "Endfire coupling between optical fibers and diffused channel waveguides," *Appl. optics*, vol. 16, no. 8, pp. 2048–2050, 1977.

[75] M. Marcuse, "Excitation of waveguides for integrated optics with laser beams," *Bell Sys. tech.*, vol. 50, pp. 43–57, 1971.

[76] C. Vassallo, "Improvement of finite-difference methods for step-index optical waveguides," *IEEE Proceedings*, vol. 139, pp. 137–142, Apr. 1992.

[77] Y. Yamamoto, T. Kamiya, and H. Yanai, "Characteristics of optical guided modes in multilayer metal-clad planar optical guide with low-index dielectric buffer layer," *IEEE Journal of Quantum Electronics*, vol. QE-11, pp. 729–736, September 1975.

[78] T. Nakano, K. Baba, and M. Miyagi, "Insertion loss and extinction ration of a surface plasmon-polariton polarizer: theoretical analysis," *Journal of Optical Society of America B*, vol. 11, pp. 2030–2035, October 1994.

[79] R. Syms and J. Cozens, *Optical Guided Waves and Devices.* Shopenhangers Road, Maidenhead, Berkshire, SL6 2QL, England: McGraw-Hill Book Company Europe, 1992.